Topaz1, an essential gene for murine spermatogenesis, down-regulates the expression of many testis-specific long non-coding RNAs.

Short title: Topaz1, long non-coding RNAs and spermatogenesis

Manon Chadourne[1], Elodie Poumerol[1], Luc Jouneau[1], Bruno Passet[2], Johan Castille[2], Eli Sellem[3], Eric Pailhoux[1] and Béatrice Mandon-Pépin[1]*

[1] Université Paris-Saclay, UVSQ, INRAE, BREED, 78350, Jouy-en-Josas, France; Ecole Nationale Vétérinaire d'Alfort, BREED, 94700, Maisons-Alfort, France.

[2] Université Paris Saclay, INRAE, AgroParisTech, GABI, Jouy-en-Josas, France.

[3] R&D Department, ALLICE, Paris, France.

* Corresponding author

E-mail: beatrice.mandon-pepin@inrae.fr (BMP)

Abstract

Spermatogenesis comprises a coordinated process, including meiosis, to produce fertile male gametes. Previous study reported that *Topaz1* is a germ cell specific gene highly conserved in vertebrates. *Topaz1* knockout male mice are sterile. The mutant testes lack haploid germ cells and meiosis arrests at the first-division prophase-metaphase transition. Here, in order to better characterize the testicular phenotype of *Topaz1*$^{-/-}$ mice, we used RNA-seq analyses at two different developmental stages. At postnatal days 16 (P16), 205 genes were differentially expressed genes (DEGs) in *Topaz1*$^{-/-}$ testes. They suggest stress conditions in mutant testes. At P18, the number of DEGs was increased 10-fold and 90% were down-regulated. The absence of *Topaz1* seems to disturb the expression of genes involved in microtubule and/or cilium mobility, spermatogenesis and first meiotic division during the transition from prophase to metaphase. This is consistent with the *Topaz1*$^{-/-}$ testis phenotype where microtubule networks and centrosomes are disrupted. Moreover, a quarter of P18-DEGs are long non-coding RNAs (lncRNAs). Three of them, down-regulated at P16 and P18, were studied. They are testis-specific, located in spermatocytes and their expression starts between P11 and P15. We report here the effects of the suppression of one of these lncRNAs, *4939463O16Rik*. The mouse fertility is not affected although the sperm parameters are disturbed. Transcriptome of P18-*4939463O16Rik*$^{-/-}$ testes is altered and the affected molecular pathways include microtubule-based process, regulation of cilium movement, spermatogenesis, male gamete differentiation. The absence of TOPAZ1 protein or of *4930463O16Rik* lncRNA showed the same enrichment clusters in mutant testes despite a contrasted phenotype on the male fertility.

In conclusion, *Topaz1* is an essential gene for male fertility in mice and seems to stabilize the expression of many lncRNAs. Its absence leads to meiotic arrest. Suppression of one lncRNA is dispensable for mouse fertility but is necessary during terminal differentiation of male gametes.

Author Summary

The *Topaz1* gene was initially characterized during the meiotic initiation in the sheep fetal ovary. In order to determine its function, the KO of the murine gene was performed. In this species, only males are sterile and spermatogenesis is blocked before the first meiotic division. Here, we show that cytoskeletal elements are strongly disturbed in mutant testes, a sign that these elements take an important function in spermatogenesis. While the mitotic spindle of spermatogonia is normal, the meiotic spindle of spermatocytes is a hemispindle-shaped and the homologous chromosome pairs cannot position themselves on the equatorial plate. In addition, lncRNAs represent 25% of genes whose testis expression varies significantly due to the absence of *Topaz1*. This suggests a key role of these factors in spermatogenesis. Largely testis specific, they could be involved in spermatogenesis with a more or less critical role on the mouse fertility, probably also depending of their redundancies.

Introduction

In mammals, an organism derived from two parental haploid gametes, a maternal oocyte and a paternal sperm. Meiosis is a highly specialized event that leads to the production of these haploid germ cells [1]. In female, meiosis is initiated during fetal life while male germ cells are involved in the meiosis process around puberty. In male, it takes place during the process of spermatogenesis that involves mitotic division and multiplication of spermatogonia, segregation of homologous chromosomes via meiosis and spermiogenesis of haploid germ cells. This complex process of spermatogenesis, which progresses through precisely timed and highly organized cycles, is primordial for male fertility. All these different events are highly regulated and associated with controlled expression of several testis-enriched genes. A previous study has shown the essential role of *Topaz1* during meiosis steps in male mice [2]. *Topaz1* is a highly conserved gene in vertebrates. Its expression is germ cell-specific, as demonstrated in mice and sheep [3]. Suppression of *Topaz1* in mice (*Topaz1*$^{-/-}$) results in males azoospermia. Male meiotic blockage occurs without deregulation of chromosome alignment and

75 TOPAZ1 is not involved in the formation of the XY body or the maintenance of MSCI. *Topaz1* depletion
76 increases apoptosis of male pachytene cells. A chromosome misalignment at the metaphasic I plate is
77 observed in the absence of *Topaz1* in mouse testes. This misalignment leads to an arrest at the
78 prophase to metaphase transition during the first meiosis division [2]. Microarray-based gene
79 expression profiling of *Topaz1*$^{-/-}$ testis revealed that TOPAZ1 influences the expression of one hundred
80 transcripts including several long non-coding RNA (lncRNAs) and unknown genes at postnatal day 20
81 (P20) [2].
82 Since the discovery of the maternal *H19* lncRNA gene [4] and of the *Xist* gene [5] that regulate the
83 structure of chromosomes and mediating gene repression during X chromosome inactivation, the
84 interest in studying the role of non-coding RNAs (ncRNAs) greatly increased. Non-coding RNAs are
85 present in many organisms, from bacteria to humans, where only 1.2% of the human genome codes
86 for functional proteins [6–8]. They are divided into two groups according to their length. The small
87 non-coding RNAs (sncRNAs) group contains transcripts smaller than 200 nucleotides (nt). They refer to
88 microRNAs (miRNAs, 20-25 nt), small interfering RNAs (siRNAs), PIWI-interacting RNAs (piRNAs, 26-31
89 nt) and circular RNAs (cricRNA) and are essential for several functions such as the regulation of gene
90 expression and genome protection (Ref in [9]). The fundamental role of sncRNAs in spermatogenesis
91 is well described in recent years [10–12]. The second group, the lncRNAs, contains transcripts longer
92 than 200 nt without significant open reading frame. Advances in high-throughput sequencing allowed
93 the identification of new transcripts, including lncRNAs. Most of them are transcribed by the RNA
94 polymerase II and possess a 5' cap and polyadenylated tail (ref in [13]). They are classified according
95 to their length, location in the genome, (surrounding regulatory elements for example) or functions.
96 While much remains to be discovered about the functions of ncRNAs and their molecular interactions,
97 accumulative evidences suggest that ncRNAs participate in various biological processes such as cell
98 differentiation, development, proliferation, apoptosis and cancers.
99 Several studies pointed out that testes have a very high proportion of lncRNA compared to other
100 organs [14,15]. However, this high testicular expression is only observed in the adult organ, as the level

101 of lncRNAs in the developing testis is comparable to somatic organs [15]. In *Drosophila*, Wen *et al*.
102 produced mutant fly lines by deleting 105 testis-specific lncRNAs and demonstrated the essential role
103 of 33 of them for spermatogenesis and/or male fertility [16]. In mice, some testis-expressed lncRNAs
104 were functionally characterized during spermatogenesis. For examples, *Mrhl* RNA repressed *Wnt*
105 signaling in the Gc1-Spg spermatogonial cell line suggesting a role in spermatocyte differentiation [17].
106 The expression of the Testis-specific X-linked gene was specific of and highly abundant in pachytene-
107 stage spermatocytes and could regulate germ cells progression in meiosis [18]. Lastly, it has been
108 shown that the *Dmrt1*-related gene negatively regulates *Dmrt1* (doublesex and mab-3 related
109 transcription factor 1) and that this regulation could be involved in the switching between mitosis and
110 meiosis in male germ cells [19].

111 Following a previous study, which presented microarray comparative analyses of wild-type and
112 *Topaz1*$^{-/-}$ testis RNAs at P15 and P20 [2], we performed a deep sequencing by bulk RNA-seq of these
113 testes collected at P16 and P18 in order to refine the developmental stages showing transcriptional
114 differences between the two mouse lines. Since the proportion of deregulated lncRNAs represented
115 about a quarter of the differentially expressed genes (DEGs), we studied the testicular localization of
116 three of them and created a mouse line deleted of one of them (*4930463O16Rik*). These knockout
117 mice showed normal fertility in both sexes, but male mutants produced half as much sperm than wild-
118 type controls.

119

120 Results

121 *Topaz1* mutant testes have a deregulated transcriptome as early as P16.

122 To expand the previous microarray comparative analyses of wild-type and mutant testis RNA
123 performed at P15 and P20, during the first wave of spermatogenesis [2], transcriptomic analyses by
124 RNA-seq were performed on WT and *Topaz1*$^{-/-}$ mouse testes at two developmental stages: P16 and
125 P18. The P16 stage was chosen because these previous microarray analyses revealed that only the

126 Topaz1 gene was expressed differently at P15, its expression starting from 5 d*pp*. This means that the
127 time when TOPAZ1 should have an effect is just after P15. Furthermore, whereas at P15, seminiferous
128 tubules contain spermatocytes that have advanced to mid and late-pachytene, at P16, they contain
129 spermatocyte cells that progressed from the end-pachytene to early diplotene of meiosis I. At P20, the
130 first round spermatids appear, whereas at P18, late-pachytene spermatocytes are abundant and the
131 very first spermatocytes II appear [20]. Thus, the two P16 and P18 stages chosen in this study
132 surrounded as close as possible the time lapse just before and after the first meiosis I division of
133 spermatogenesis.
134
135 Differential analyses of RNA-seq results showed that 205 and 2748 genes were significantly
136 deregulated in *Topaz1*$^{-/-}$ testis compared to WT at P16 and P18 respectively (adjust p-value < 0.05 and
137 absolute Log2 Fold Change > 1 (Log2FC>1) (Fig 1A, S1 Table). At P16, out of the 205 DEGs, 97 genes
138 were significantly down-regulated (Log2FC<-1 or FC<0.5) and 108 up-regulated (Log2FC>1 or FC>2).
139 However, at P18 down-regulated DEGs accounted for 91% (2491 genes) and up-regulated genes for
140 only 9% (257genes). Among all these DEGs, 120 were in common between P16 and P18 (Fig 1A). The
141 2748 DEGs of the developmental stage P18 were largely testis-enriched DEGs in mouse testis specific
142 genes according to the mouse gene atlas (Fig 1B).

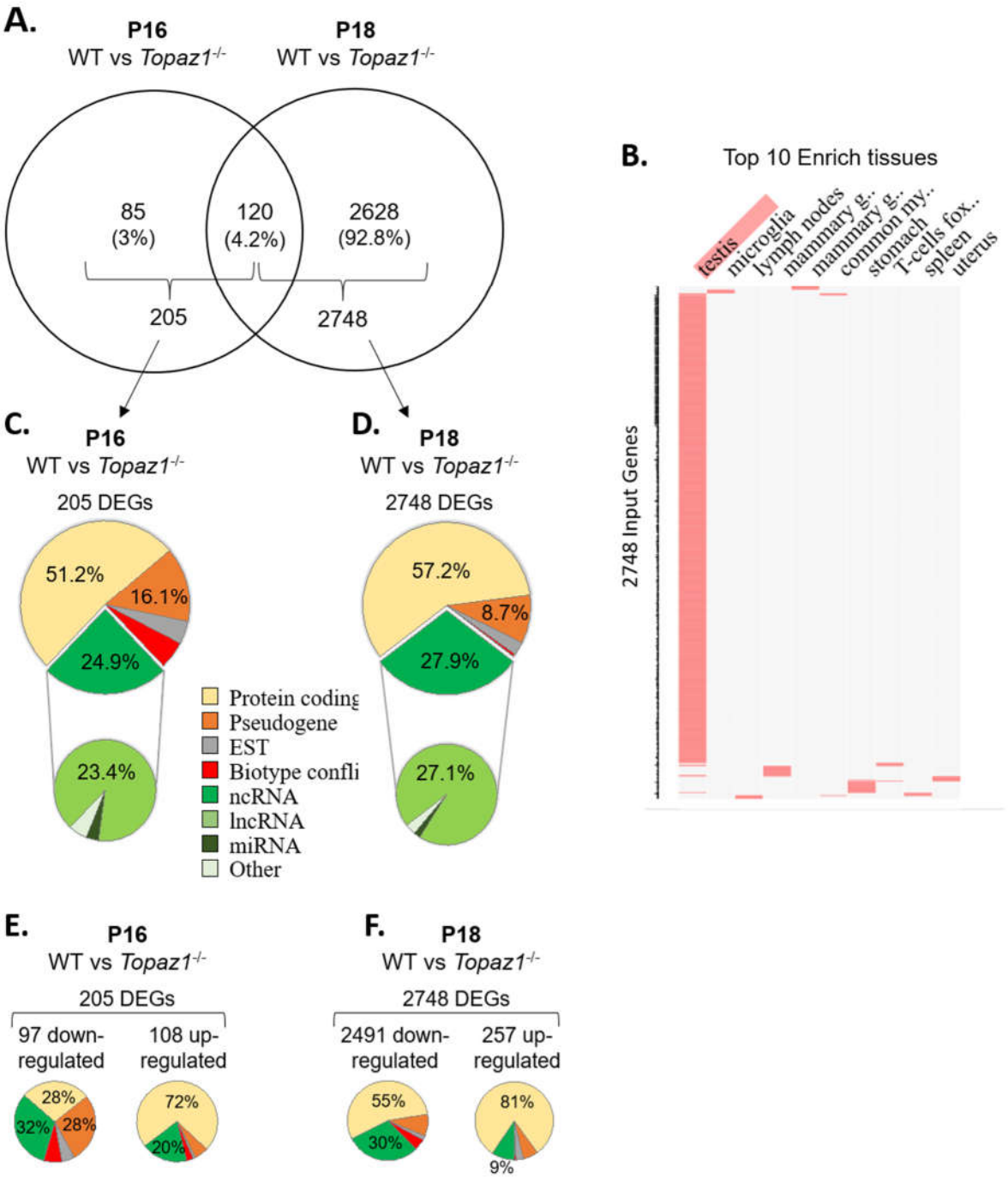

143

144 **Fig 1: WT vs *Topaz1*$^{-/-}$ deregulated gene analysis from mouse testes.**

145 (A) Venn diagram showing overlap of differentially expressed genes between P16 and P18 *Topaz1*$^{-/-}$ mouse testes

146 (adj p<0.05 and down-regulated FC<0.5 (log2FC<-1) or up-regulated FC>2 (log2FC>1)). (B) Clustergrammer was

147 generated by the Enrichr website. Top 10 enrich tissues are the columns, input genes (2748 DEGs of P18 *Topaz1*$^{-}$

148 $^{/-}$ compared to normal testes) are the rows, and cells in the matrix indicate if a DEG is associated with a tissue

149 from the Mouse Gene Atlas. (C-D) Biotype of DEGs in *Topaz1*$^{-/-}$ testis of (C) P16 and (D) P18. Around half of them

150 are protein-coding genes whereas around one quarter is ncRNA at both developmental stages. (E-F) Biotype of
151 DEGs in *Topaz1*$^{-/-}$ testis of (E) P16 and (F) P18 depending on whether they were up- or down-regulated.
152
153 Validation of several DEGs was realized by RT-qPCR. Two randomly selected up-regulated genes at P16
154 (B3galt2 and Hp) and three at P18 (*B3galt2*, *Afm* and *Cx3cr1*), four down-regulated genes at P16 and
155 P18 (*Gstt2*, *4930463O16Rik*, *4921513H07Rik* and *Gm21269*) and two non-differential genes (*Cdc25c*
156 and *Nop10*) were analyzed (S1 Fig). Results confirmed those obtained by RNA-seq.
157 The biotype of the differential transcripts (protein-coding, non-coding RNAs…) was performed on the
158 annotation of the NCBI, MGI and Ensembl databases. Two major deregulated groups were highlighted
159 at both stages. The protein-coding gene biotype accounted for half of the deregulated genes (51.2%
160 and 57.2% at P16 and P18 respectively) (Fig 1C-D). A quarter of *Topaz1*$^{-/-}$ DEGs, 24.9% and 27.9% at
161 P16 and P18 respectively, was found to belong to the ncRNA second group. Among this latter one, the
162 major biotype was the lncRNAs one at both stages, 23.4% and 27.1% at P16 and P18 respectively. This
163 significant proportion of deregulated lncRNA raises the question of their potential involvement in
164 spermatogenesis.
165
166 **Pathway and functional analysis of DEGs**
167 To further understand biological functions and pathways, these DEGs were functionally annotated
168 based on GO terms and KEGG pathway or on InterPro databases through the Database for Annotation,
169 Visualization and Integrated Discovery ontology database (DAVID v6.8, https://david.ncifcrf.gov/) with
170 the default criteria [21,22].
171 At P16, thus before the first meiosis division, out of 205 differentially expressed genes, 32% of down-
172 and 20% of up- regulated genes corresponded to non-coding RNAs with no GO annotation or no
173 pathway affiliation for the vast majority (Fig 1E), leading a less powerful functional annotation
174 clustering (S2 Table). Five clusters with an enrichment score > 1.3 were obtained (enrichment score >
175 1.3 was used for a cluster to be statistically significant as recommended by Huang et al., [21] but the

176 number of genes in each cluster was low except for the Annotation cluster number 4. In this one,
177 TOPAZ1 absence seems to affect the extracellular compartment. The others referred to the antioxidant
178 molecular function and the detoxification biological process, suggesting stress conditions.
179 At P18, corresponding to the first transitions from prophase to metaphase, either considering all DEGs
180 (2748 DEGs; 2404 DAVID IDs) or only the down-regulated genes (2491 DEGs; 2164 DAVID IDs) in the
181 P18 *Topaz1*$^{-/-}$ versus WT testes, resulted in the identification of five identical clusters with an
182 enrichment score higher than 12 (Fig 1F, S3 Table). However, enrichment scores were higher when
183 only the down-regulated genes were considered. These clusters include the following GO terms (*i*) for
184 cellular components: motile cilium, ciliary part, sperm flagellum, axoneme, acrosomal vesicule; (*ii*) for
185 biological processes: microtubule-based process, spermatogenesis, germ cell development, spermatid
186 differentiation (S3 Table).
187 Finally, using the InterPro database, four clusters with enrichment score > 1.3 were obtained based on
188 down-regulated genes (S3 Table) and with-up-expressed genes, the absence of TOPAZ1 in mouse testes
189 highlighted the biological pathway of the response to external stimulus or of the defense response in
190 the testis, again suggesting, as for P16, stressful conditions in these *Topaz1*$^{-/-}$ testes.
191 These results indicated that the absence of TOPAZ1 induced alterations of the murine transcriptome
192 of mutant testis transcriptome as early as 16 days after birth. Two days later (P18), these effects were
193 amplified and with a predominantly down-regulation of genes (91% of DEGs). The loss of TOPAZ1
194 appeared to disrupt the regulation of genes involved in microtubule and/or cilium mobility,
195 spermatogenesis and first meiotic division during the prophase to metaphase transition. This is in
196 agreement with the *Topaz1*$^{-/-}$ phenotype in testes.
197

198 **Absence of TOPAZ1 leads to drastic cytoplasmic defects before the first meiotic division**

199 According to the preceding GO pathway analyses showing that a majority of deregulated proteins are
200 involved in microtubule cytoskeleton organization, microtubule-based movements and processes,
201 microtubule organizing centers, centrosomes and centrioles in P18 Topaz1$^{-/-}$ testes (S3 Table), we

202 aimed to better characterize the cytoplasmic components of germ cells in Topaz1$^{-/-}$ testes before the
203 first meiotic division. As the meiotic spindle is a key component of these cells before and during the
204 metaphase stage, we studied it by α- and γ-tubulin immunofluorescence (IF) staining, markers of
205 microtubule spindle and centrosome respectively (Fig 2). We observed a hemispindle centered in the
206 germ cells of the Topaz$^{-/-}$ testis. Moreover, in these cells, centrosome staining was diffuse and weak.
207 This was also observed on entire seminiferous sections (S2 Fig). The chromosomes were not aligned
208 along a metaphase plate but adopted an atypical rosette shape (Fig 2), reflecting a strong perturbation
209 of the microtubule and centrosome pathways in Topaz1-deficient spermatocytes that leads to meiotic
210 arrest.

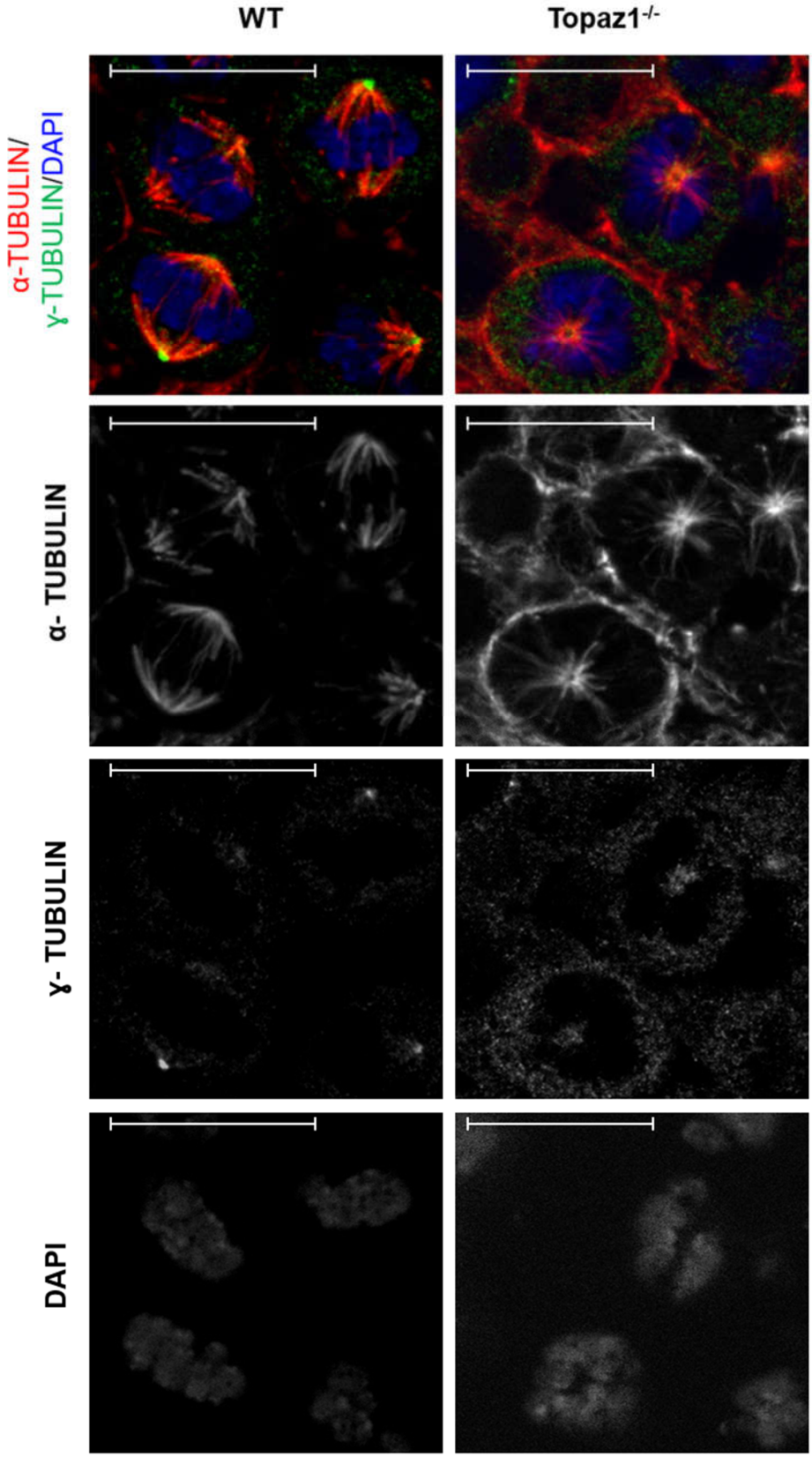

211

212 **Fig 2: Abnormal metaphase phenotype in Topaz1-deficient gonads.**

213 Immunofluorescence staining for α-TUBULIN (red), γ-TUBULIN (green) and DAPI (blue) in WT (left) and Topaz1$^{-/-}$
214 (right) 28 d*pp* testis sections. Unlike meiotic metaphases seen in normal testes (left), metaphases are abnormal
215 in Topaz1$^{-/-}$ mutants (right) with atypical rosette shape and hemispindle. Scale bar = 20µm
216

217 **Selection of 3 deregulated lncRNA: all spermatocyte-specific**

218 The vast majority of deregulated lncRNAs in *Topaz1*$^{-/-}$ testes has an unknown function. We decided to
219 study 3 of the 35 down-regulated lncRNAs that are shared by P16 and P18 stages, namely
220 *4930463O16Rik* (ENSMUSG00000020033), *4921513H07Rik* (ENSMUSG00000107042) that is the most
221 down-regulated gene at P16 with a Log2FC of 11.85, both already highlighted in the previous
222 microarray comparative analyses [2] and *Gm21269* (ENSMUSG00000108448), that has the lowest
223 adjust p-value at P18. We quantified these transcripts by qPCR in several somatic tissues (brain, heart,
224 liver, lung, small intestine, muscle, spleen, kidney, epididymis and placenta) and in gonads (testis and
225 ovary). These three lncRNAs were almost exclusively expressed in testis (Fig 3A, C, E). These results
226 were in agreement with RNA-seq data available for *4930463O16Rik* and *Gm21269* on the
227 ReproGenomics viewer (https://rgv.genouest.org/) (S3A and S4A Figs respectively) [23,24]. Our RNA-
228 seq results, summarized using our read density data (bigwig) and the Integrative Genomics Viewer
229 (IGV; http://software.broadinstitute.org/software/igv/), showed a weak or absence of expression of
230 these three genes in *Topaz1*$^{-/-}$ testes (S5A-C Fig).

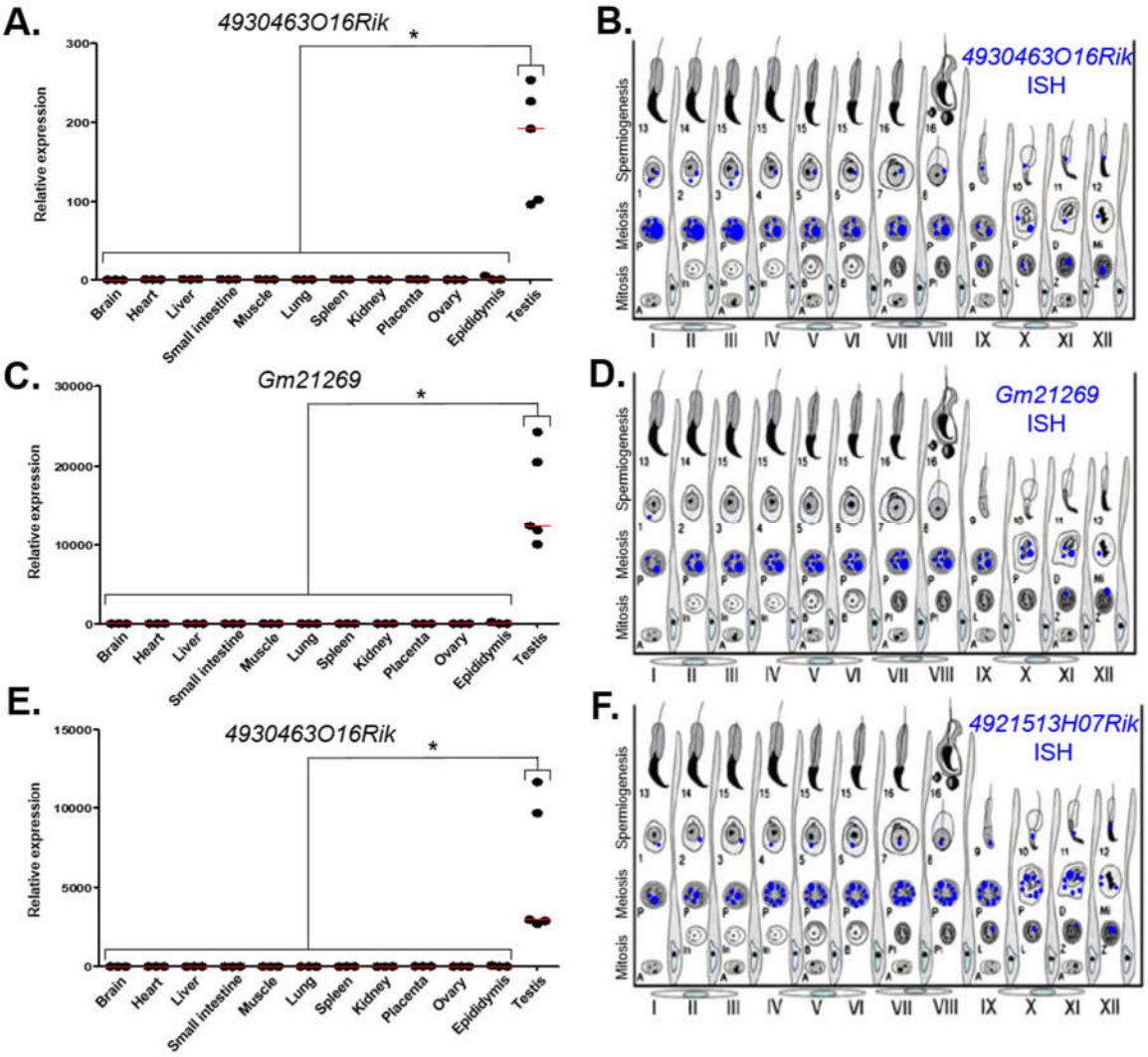

231

232 **Fig 3: Expression analysis of three lncRNAs.**

233 (A-C-E) RT-qPCR analysis of three different lncRNAs. (A) *4930463O16Rik*; (C) *Gm21269*; (E) *4921513H07Rik* in

234 different two month-old tissues of WT mice. The red lines represent the median for each tissues. n=5 for testes

235 and n=3 for other organs. Statistical analyses were realized with non-parametric Kruskal-Wallis test. * = $p<0.05$

236 (B-D-F) Schematic representation of the result of (B) *4930463O16Rik*, (D) *Gm21269* and (F) *49215113H07Rik ISH*

237 expression in the meiotic and post-meiotic cells of the WT mouse seminiferous epithelial cycle.

238

239 Quantification of these transcripts by qPCR from postnatal to adulthood in WT and *Topaz1*$^{-/-}$ testes

240 was previously reported, as for *4930463O16Rik* and *4921513H07Rik* (Fig 9 in [2]) or realized for

241 *Gm21269* (S6 Fig, also including the postnatal expression of *4930463O16Rik* and *4921513H07Rik*). The

242 difference of expression between normal and *Topaz1*$^{-/-}$ testes was detected significantly as early as
243 P15 (detected insignificant in the previous microarray analysis and *Gm21269* was absent on the used
244 microarray). All showed an absence of expression or at least an important down-regulation in the
245 mutant testis.
246
247 To determine testicular localization of these lncRNA, *in situ* hybridization (*IS*H) on adult WT testis
248 sections was performed (S7 Fig) and results summarized (Fig 3B, D, F). These lncRNAs were expressed
249 in spermatocytes and the most intense probe labeling was observed in the pachytene stage. These
250 results were confirmed by data on the ReproGenomics viewer for *4930463O16Rik* and *Gm21269*
251 (https://rgv.genouest.org/) (S3B and S4B Figs) [23,24].
252 To refine the subcellular localization of these transcripts in the adult mouse testis, we have paired *IS*H
253 experiments and IF staining of the DDX4 protein (or Mvh, Mouse Vasa homolog). DDX4 is a germ cell
254 cytoplasmic marker of germ cells, especially in the testis [25]. Our results showed that the three
255 observed lncRNAs had different expression intensities depending on seminiferous epithelium stages.
256 *4930463O16Rik* was expressed in the nucleus of spermatocytes with a diffuse fluorescence,
257 surrounded by the cytoplasmic DDX4 labelling from the zygotene to the diplotene stages (Fig 4A-B-C).
258 In the same spermatocyte stages (zygotene to diplotene), diffuse labelling of *Gm21269*, similar to that
259 of *4930463O16Rik*, was observed but with the addition of a dot-shaped labelling that co-localized with
260 DDX4 fluorescence (Fig 4D, E, F). *Gm21269* was therefore localized in the cytoplasm and nuclei of
261 spermatocytes during meiosis. *4921513H07Rik* seemed to be cytoplasmic with fluorescent red dots
262 (*IS*H) surrounding the nuclei, and located in close proximity of DDX4 (IF) labelling (Fig 4G, H, I). In other
263 stages, identified by DDX4 staining, *IS*H labelling of these three lncRNA resulted in the observation of
264 single dots in a few spermatogonia and in round spermatids. We performed the same experiment: *IS*H
265 was followed by an IF staining of γH2Ax to highlight the sex body in spermatocytes (S8 Fig). No co-
266 localization between the sex body and the three lncRNA was revealed.

267 Altogether, these results suggested that these spermatocyte-specific lncRNAs had different subcellular

268 localization into spermatocytes, suggesting functions in these male germ cells.

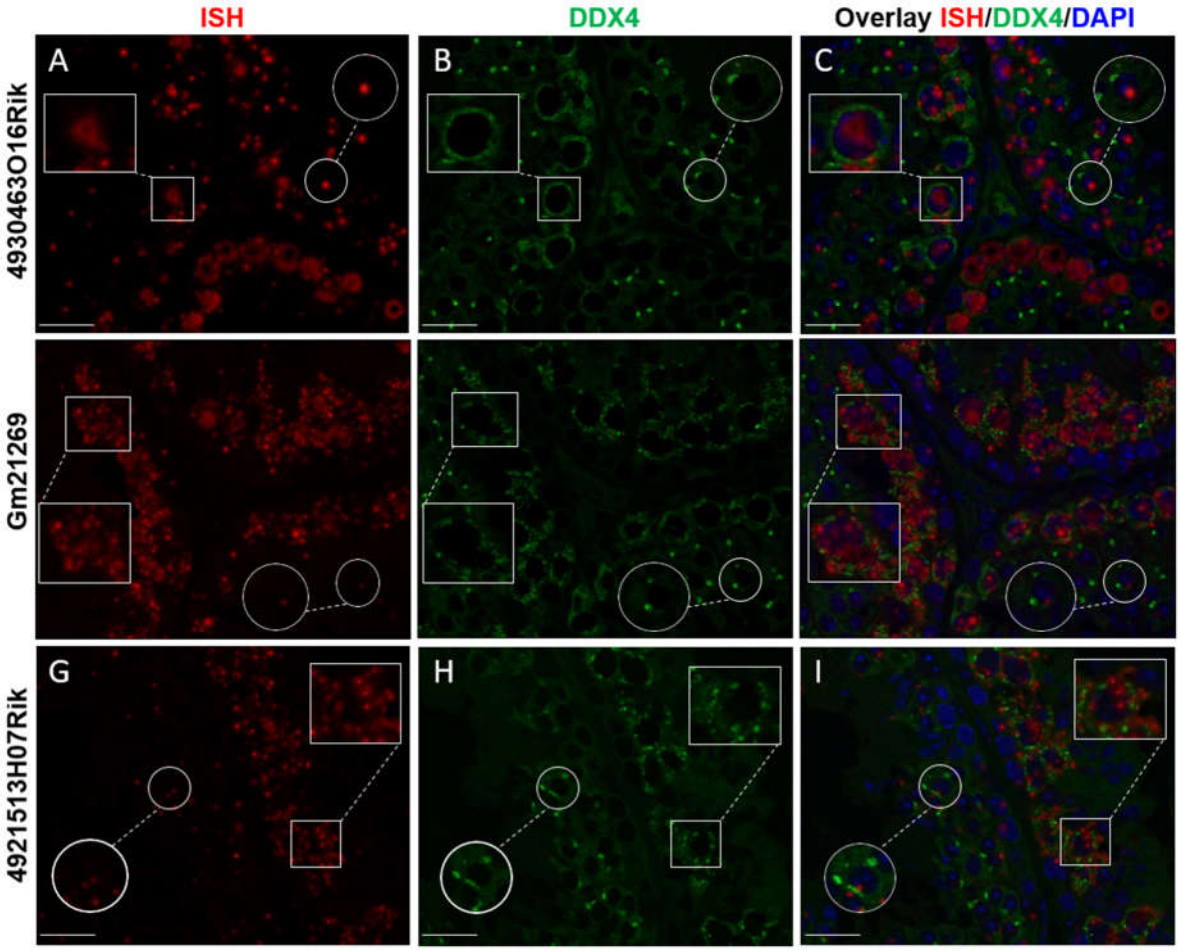

269

270 **Fig 4: lncRNA cellular localizations on WT two month-old mouse testes.**

271 In situ hybridization using (A) *4930463O16Rik*, (D) *Gm21269* and (G) *4921513H07Rik* probes (red). (B-E-H)

272 Immunofluorescence staining with DDX4 antibody was achieved in the same stage of seminiferous epithelium to

273 identify male germ cells (green). (C-F-I) DAPI (blue), visualizing nuclear chromosomes, was merge with *IS*H (green)

274 and IF (red) signals. Zooms in white squares showed spermatocytes during first meiotic division (zygotene to

275 diplotene stages). Zooms in circles showed spermatid cells with one spot of DDX4 staining per cell. Scale bar =

276 20 µm.

277

278 **Generation of *4930463O16Rik*-deleted mice**

279 In order to evaluate a potential role in spermatogenesis of one of these lncRNAs, *4930463O16Rik*, the
280 nuclear expressed gene, was chosen to suppress its expression in a mouse knockout model.
281 *4930463O16Rik* gene (Chr10: 84,488,293-84,497,435 - GRCm38:CM001003.2) was described in public
282 databases as consisting of 4 exons spanning approximately 10 kb in an intergenic locus on the mouse
283 chromosome 10. By PCR and sequencing, we confirmed this arrangement (data not shown). In the goal
284 of understand the role of *4930463O16Rik*, a new mouse line deleted of this lncRNA was created by
285 CRISPR/Cas9 technology (Fig 5A). Briefly, multiple single guide RNAs (sgRNAs) were chosen, 2 sgRNAs
286 in 5' of exon 1 and 2 sgRNAs in 3' of exon 4, to target the entire length of this gene (Fig 5A, C) and
287 increase gene deletion efficiency in mouse [26]. Mice with disruption of the target site were identified
288 after Sanger sequencing of PCR amplification of the genomic region surrounding the deleted locus (Fig
289 5D). *4930463O16Rik*$^{+/-}$ mice were fertile and growth normally. Males and females *4930463O16Rik*$^{+/-}$
290 were mated to obtain *4930463O16Rik*$^{-/-}$ mice. Once the mouse line was established, all pups were
291 genotyped with a combination of primers (listed in S4 Table) (Fig 5B).

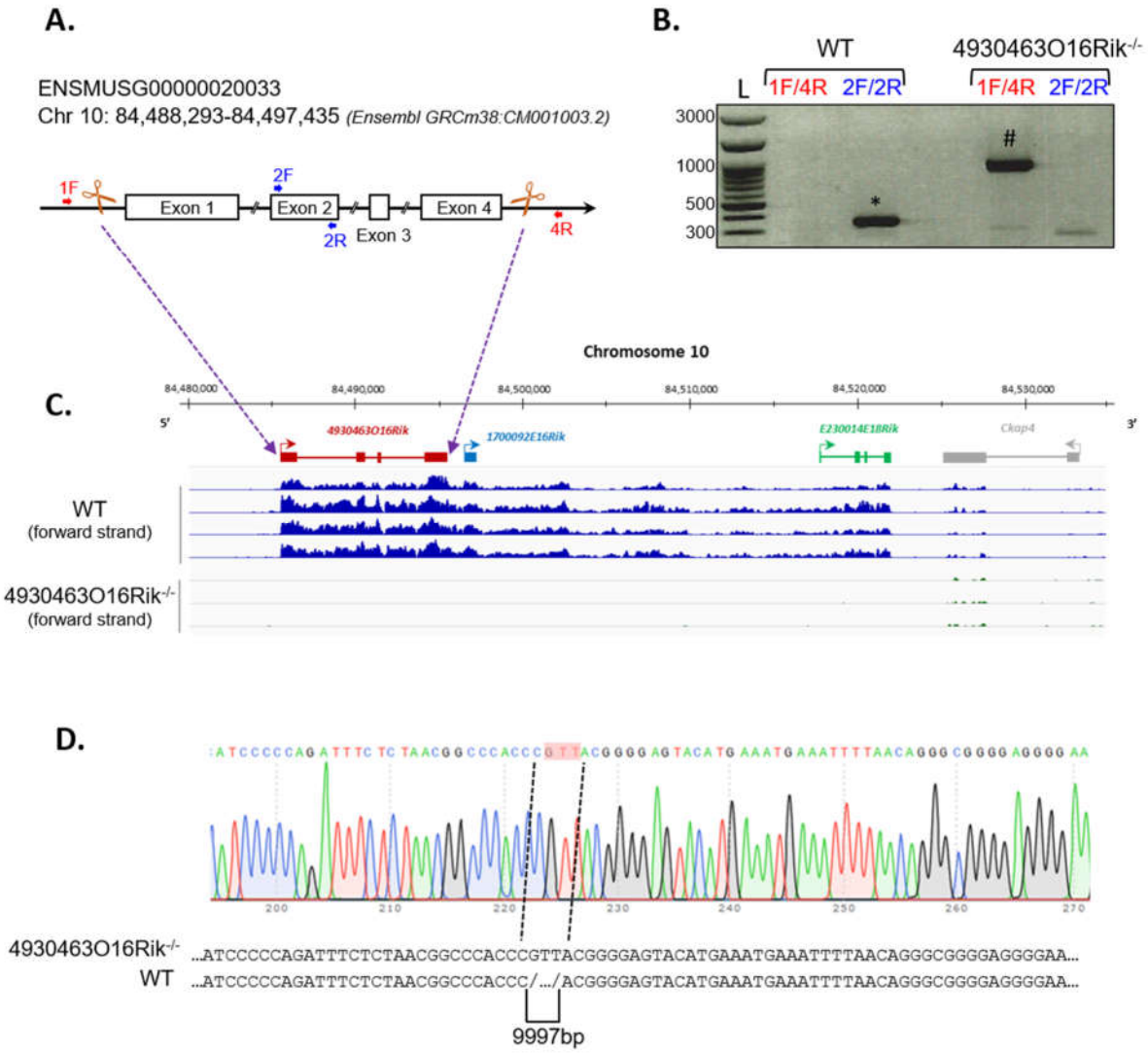

Fig 5: Deletion of the *4930463O16Rik* gene in mouse.

(A) Schematic design of the CRISPR/Cas9 deletion of the *4930463O16Rik* gene with suppression of the 4 exons and 3 introns. The white boxes and lines represent exons and introns, respectively. (B) PCR genotyping on DNA of WT and *4930463O161Rik*$^{-/-}$ mice. The primer pairs used 1F/4R (located in 5' of exon 1 and in 3' of exon 4 of the *4930463O16Rik* gene respectively) or 2F/2R (located in the exon2 of *4930463O16Rik*) were used to determine the genotype of mice. Results showed the following amplicon sizes: (*) 352 bp with the 2F/2R primers in WT (no amplification in mutant mice); (#) 935 bp with the 1F/4R primers on *4930463O161Rik*$^{-/-}$ mice (no amplification in WT mice in the PCR conditions used). (L) DNA ladder. (C) Transcription of the forward strand of chromosome 10 around *4930463O16Rik* gene with RNA-seq coverage (BigWig format representation) in WT (top blue tracks) and *4930463O16Rik*$^{-/-}$ (bottom tracks) mouse P18-testes. A continuous (WT) or very low transcription (*4930463O16Rik*$^{-/-}$) was observed from *4930463O16Rik* until *E230014E18Rik* genes. (D) Electrophoregramm of

304 *4930463O16Rik*$^{-/-}$ mouse genomic DNA showing 9997 bp deletion and an insertion of 3 nucleotides (GTT,
305 highlighted in pink).
306
307 **The absence of *4930463O16Rik* does not affect mouse fertility**
308 Fertility was investigated in *4930463O16Rik* deficient mice. Eight-week-old males and females
309 *4930463O16Rik*$^{-/-}$ mice were matted. *4930463O16Rik*$^{-/-}$ mice were fertile in both sexes. Their litter size
310 (7.5 ± 2.10 pups per litter, n=28) was similar to that of their WT counterparts (6.9 ± 2.12 pups per litter,
311 n=20). There was no significant difference in testicular size, in morphology and histology of testis,
312 cauda and caput epididymis between WT and *4930463O16Rik*$^{-/-}$ adult mice (Fig 6A, B). In addition, the
313 different stages of seminiferous tubules divided into seven groups were quantified between
314 *4930463O16Rik*$^{-/-}$ and WT adult mice. No significant difference was observed between both genotypes
315 (Fig 6C). These results demonstrated that *4930463O16Rik* is not required for mouse fertility.

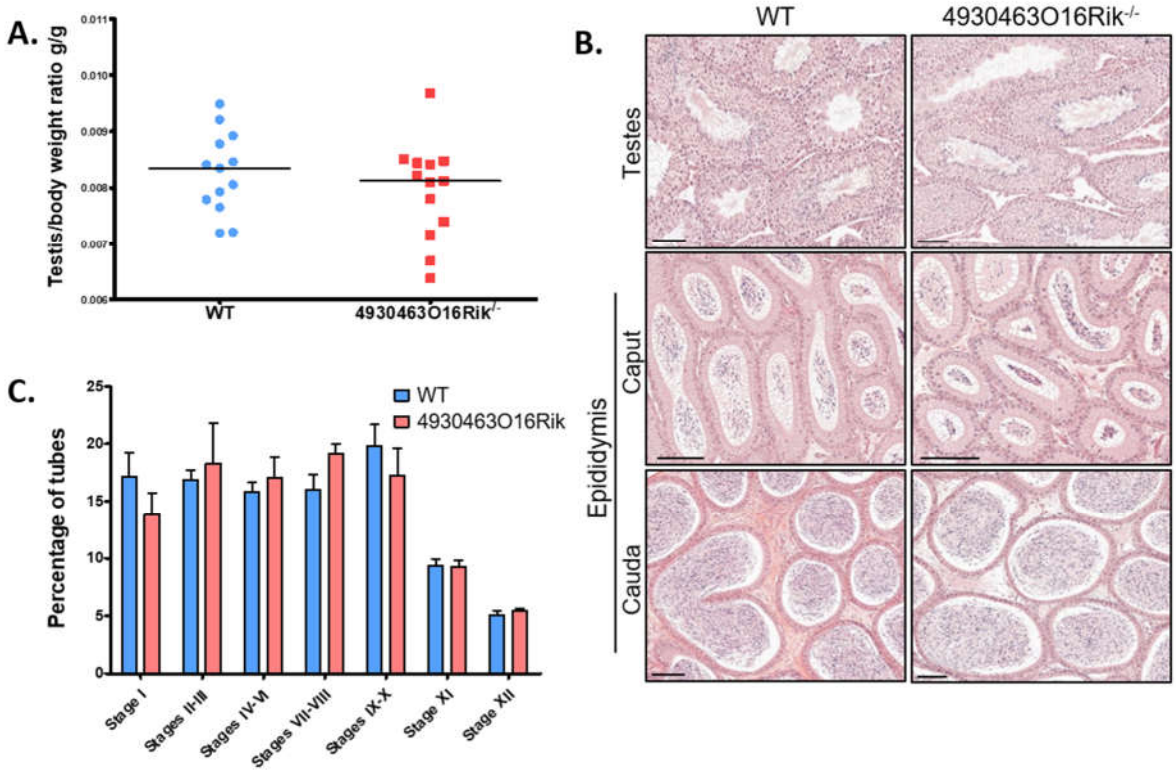

316
317 **Fig 6: Study of *4930463O16Rik*$^{-/-}$ testicular phenotype.**

318 (A) Testis/body weight ratio of 8 week-old mice. No significant difference was observed in both mouse lines.
319 Median lines were in black. (B) Haematoxylin and eosin (HE) staining of testis and epididymis sections from WT
320 and *4930463O16Rik*$^{-/-}$ 8 week-old mice. Scale bar=50 µm. Spermatozoa were visible in the lumen of the testis
321 and epididymis of WT and *4930463O16Rik*$^{-/-}$. (C) Quantification of the different seminiferous epithelium stages
322 in WT and *4930463O16Rik*$^{-/-}$ 8 week-old mice. No significant difference was found between WT and
323 *4930463O16Rik*$^{-/-}$ mice.
324

325 **_4930463O16Rik_$^{-/-}$ mice present modified sperm parameters**

326 Sperm parameters in 8-week-old testis lacking *4930463O16Rik* were compared to WT testis of the
327 same age. Sperm concentration obtained from epididymis of *4930463O16Rik*$^{-/-}$ mice was significantly
328 reduced by 57.2% compared to WT (Fig 7A) despite an unmodified testis/body weight ratio (Fig 6A).
329 Motility parameters such as the percentage of motile spermatozoa, the motile mean expressed as beat
330 cross frequency (bcf) and the progressive spermatozoa were significantly higher in *4930463O16Rik*$^{-/-}$
331 mice compared to WT (Fig 7B, C, D). From a morphological point of view, two parameters were
332 significantly modified in the testis of mutant mice: the distal mid-piece reflex (DMR), a defect
333 developing in the epididymis and attesting of the sperm tail abnormality [27] and the percentage of
334 spermatozoa with coiled tail (Fig 7E, F). In addition, two kinetic parameters were also significantly
335 reduced in mutant sperm: the motile mean vsl, related to the progressive velocity in straight line) and
336 the average path velocity, or vap (Fig 7G, H).

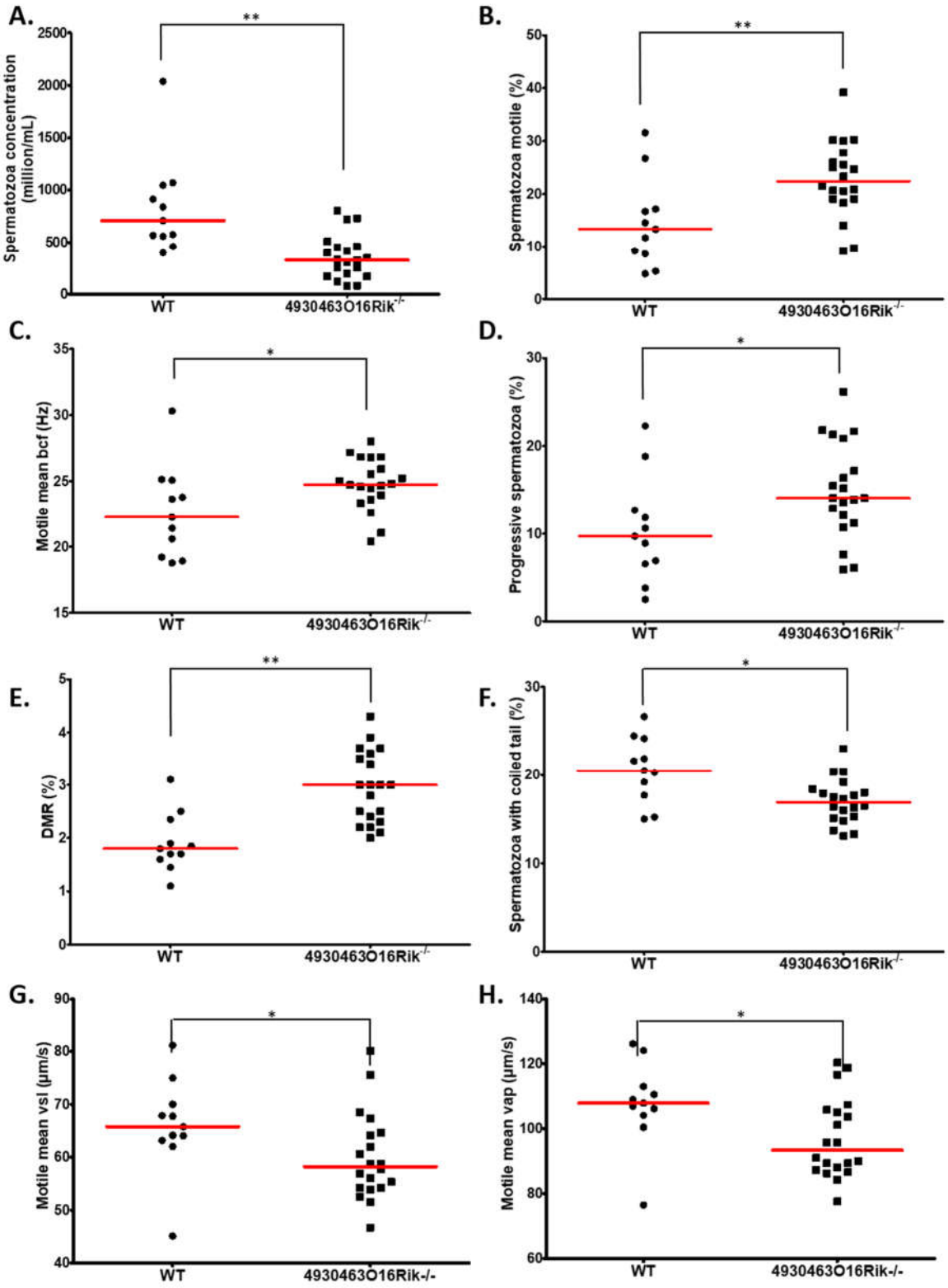

Fig 7: Evaluation of sperm parameters.

Comparison of sperm-specific parameters from WT (circle, n=11) and *4930463O16Rik*$^{-/-}$ (square, n=20) mice. Significantly affected sperm parameters were (A) spermatozoa concentration (10^6/mL), (B) spermatozoa motility

341 (%), (C) motile mean bcf (beat cross frequency), (D) progressive spermatozoa (%), (E) DMR (distal midpiece reflex,
342 abnormality of the sperm tail, %), (F) spermatozoa with coiled tail (%), (G) motile mean VSL (µm/s) and (H) VAP
343 (µm/s). Statistical analyses were realized with non-parametric Kruskal-Wallis test. * = p-val<0.05, ** = p-val<0.01.
344
345 These results showed that several sperm parameters, namely concentration, motility, morphology and
346 kinetics, were impacted by computer-aided sperm analysis (CASA) in the *4930463O16Rik* lncRNA-
347 deficient mice. Some of them would suggest negatively impacting fertility, as the sperm concentration,
348 the DMR, the percentage of coiled tail, the motile mean vsl while others would rather suggest
349 increased fertility, such as the motile mean percentage and bcf, the progressive spermatozoa. These
350 observations might explain the resulting normal fertility of *4930463O16Rik* lncRNA-deficient mice.
351
352 **Normal male fertility despite *4930463O16Rik*$^{-/-}$ mouse testis transcriptome modified**
353 Transcriptomic RNA-seq analyses were performed in WT and *4930463O16Rik*$^{-/-}$ mouse testes at two
354 developmental stages: P16 and 18, as in the *Topaz1*$^{-/-}$ mouse line.
355 At P16, seven genes were differentially expressed (adjust p-value<0.05; absolute Log2FC>1) among
356 which, *4930463O16Rik*, but also *1700092E16Rik* and *E230014E18Rik* (S5 Table). These observations
357 reinforced our hypothesis that these last two Riken cDNAs are in fact in the 3' transcribed RNA of
358 *4930463O16Rik* (positioned in Fig 5C) and correspond to a unique locus. Transcriptional activity of this
359 new locus stops towards the 3' end of the *cKap4* gene (cytoskeleton-associated protein 4 or Climp-63).
360 This gene was down-regulated by 1.7 fold in both knock-out lines (*Topaz1* and *4930463O16Rik*). This
361 could suggest a newly discovered positive regulatory role of this lncRNA on the *cKap4* gene.
362 At P18, 258 genes were differentially expressed (199 down- and 59-up regulated using same statistical
363 parameters, S5 Table). Among them, 206 were protein-coding genes representing 79.8% of DEGs (Fig
364 8A). Thus, P18 DEGs highlighted a direct or indirect relationship between the loss of the
365 *4930463O16Rik* lncRNA and protein-coding genes. In addition, the loss of this lncRNA also resulted in
366 the deregulation of 37 (14.3%) other lncRNAs.

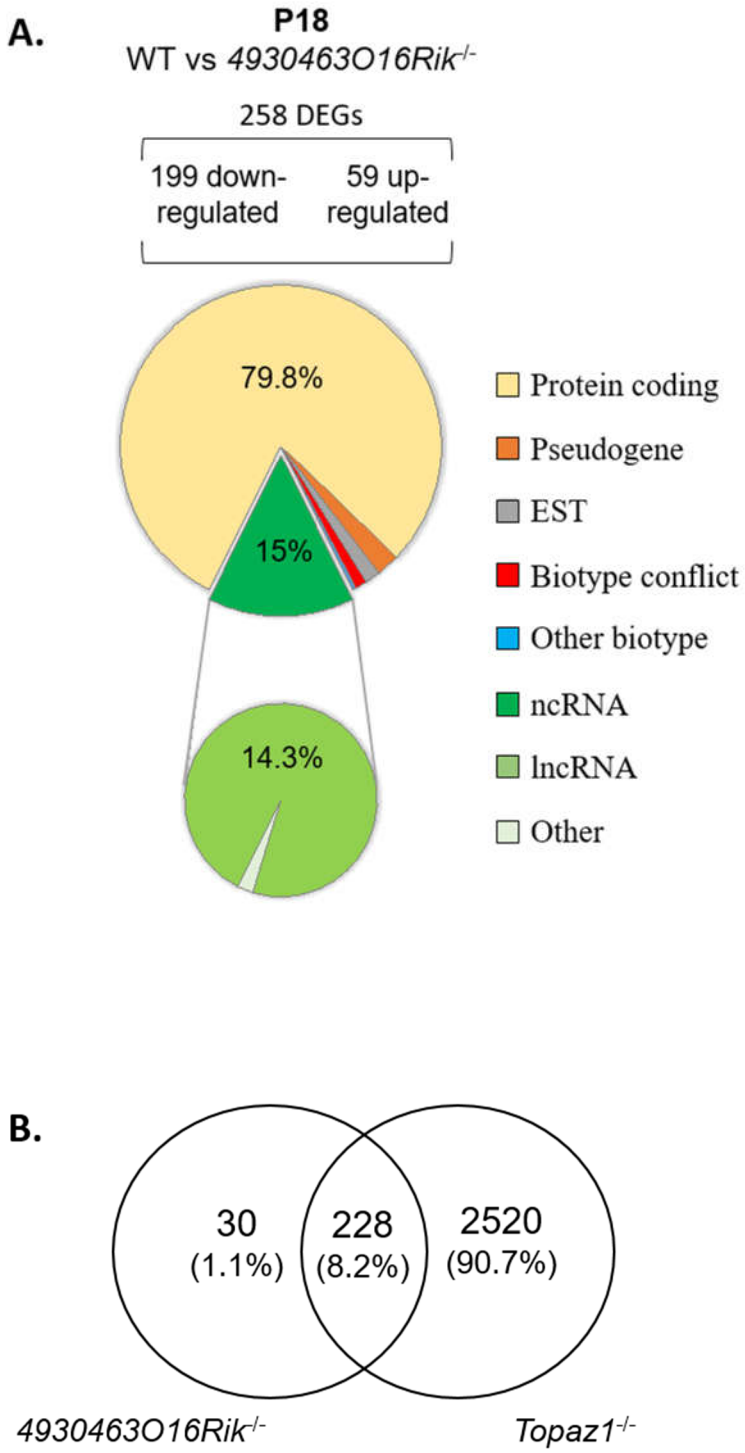

Fig 8: Deregulated genes from *4930463O16Rik*$^{-/-}$ mouse testes.

(A) Biotype of differential expressed gene at P18 in *4930463O16Rik*$^{-/-}$ testis. Most of deregulated gene are coding protein genes (adj $p<0.05$ and down-regulated FC<2 (log2FC<-1) or up-regulated FC>2 (log2FC>1). (B) Venn

371 diagram showing overlap of differentially expressed genes between *4930463O16Rik*$^{-/-}$ and *Topaz1*$^{-/-}$ mouse testes
372 at 18 d*pp*.
373
374 Validation of several DEGs was performed by RT-qPCR using WT and *4930463O16Rik*$^{-/-}$ testicular RNAs
375 of both developmental stages (P16 and P18) (S9 Fig). The qPCR results for the genes tested were
376 consistent with those of RNA-seq.
377
378 The *4930463O16Rik*$^{-/-}$ DEGs were also analyzed with the DAVID database (S6 Table). At P18, six
379 functional clustering have an enrichment score > 1.3 [21]. As for *Topaz1*$^{-/-}$ mouse testis, they included
380 the following GO terms (*i*) for cellular components: cilium movement, ciliary part, axoneme; (*ii*) for
381 biological processes: microtubule-based process, regulation of cilium movement, spermatogenesis,
382 male gamete generation, spermatid development and differentiation (S6 Table). Analyzing by
383 discriminating up- from down-regulated genes only increased the value of the enrichment score for
384 the down-regulated genes. The absence of TOPAZ1 protein or of *4930463O16Rik* lncRNA showed the
385 same enrichment clusters in mutant testes despite different outcomes on the fertility of male mice.
386 The other clusters from the DAVID analysis referred to the GO terms: cell surface, external side of
387 membrane, defense or immune response and response to external stimulus .These clusters were only
388 found in DAVID analysis with up-regulated genes.
389 Therefore, *4930463O16Rik* gene would appear to regulate genes related to spermatogenesis,
390 microtubule or cil organizations and cytoskeleton in the P18 testis. In the absence of this lncRNA, some
391 genes involved in defense mechanisms or immune response are also deregulated suggesting stressful
392 conditions. It should be noted that the majority (228/258 or 88%) of the DEGs from P18-
393 *4930463O16Rik*$^{-/-}$ testis was in common with those deregulated in *Topaz1*$^{-/-}$ mice (Fig 8B). This led to
394 similar results on ontological analyses of the DEGs of the two mutant lines. These 228 genes could be,
395 in the *Topaz1*$^{-/-}$ testes, a consequence of the down-regulation of the *4930463O16Rik* lncRNA. On the
396 other hand, these 228 DEGs alone do not explain the meiotic arrest in the *Topaz1*$^{-/-}$ testes.

397

398 ## Discussion

399 *Topaz1* was initially reported as a germ-cell specific factor [3], essential for meiotic progression and
400 male fertility in mice [2]. Suppression of *Topaz1* led to an arrest of meiosis progression at the diplotene-
401 metaphase I transition associated with germ cell apoptosis. Moreover, a first transcriptomic approach,
402 based on DNA microarrays, allowed observing a large but not exhaustive repertoire of deregulated
403 transcripts. With this technology, 10% of differentially probes were lncRNAs and presented a
404 deregulated expression in P20 *Topaz1*$^{-/-}$ testes compared to WT.
405 In this study, we show that the effects of the absence of the *Topaz1* gene are visible on the mouse
406 testicular transcriptome as early as 16 days *post-partum*, i.e. before the first meiotic division and the
407 production of haploid germ cells. These effects are amplified at 18 days post-natal, just before or at
408 the very beginning of the appearance of the first haploid germ cells. The molecular pathways involved
409 in the suppression of Topaz1 belong to spermatogenesis and to the establishment of the cell
410 cytoskeleton. At these two stages, P16 and P18, about a quarter of the deregulated genes in testes are
411 ncRNAs, mainly lncRNAs, some of which show almost no expression in *Topaz1*$^{-/-}$ testis. Suppression of
412 one of them does not prevent the production of haploid spermatids and spermatozoa, but halves the
413 murine sperm concentration. Furthermore, by deleting ~10 kb corresponding to this *4930463O16Rik*
414 lincRNA, we show that the transcriptional extinction is even longer, encompassing ~35 kb in total and
415 two other genes (1700092E16Rik (unknown gene type according to Ensembl) and the lincRNA
416 E230014E18Rik). Our transcriptional data suggest in fact that these three annotated loci belong to a
417 unique gene. Transcription of this lincRNA ended near the 3' region of the *cKap4* gene, a gene known
418 to be associated with the cytoskeleton [28]. Remarkably, cKap4 expression is down-regulated by 1.7
419 fold in both knockout mice (*Topaz1*$^{-/-}$ and *4930463O16Rik*$^{-/-}$), suggesting a previously unknown positive
420 regulatory role of *4930463O16Rik* on *cKap4*.
421

422 **TOPAZ1 ablation leads to chromosome misalignments at pro-metaphase I.**

423 Meiosis and its two cell divisions are well-orchestrated sequences of events controlled by different
424 genes. Although these divisions have many similarities between males and females, meiosis is also sex-
425 dimorphic. This particularly concerns timing, synchronization, the number of haploid gametes
426 produced and the periods of meiotic arrest (reviewed by [29]). In females, meiosis is initiated during
427 fetal life and the development of oocytes is arrested at the end of prophase I. Oocytes remain in this
428 arrested state until the onset of ovulatory cycles around puberty. There, the first division of meiosis
429 resumes and leads to the release of a first polar globule with the secondary oocyte. At metaphase II,
430 the oocyte is blocked again. The release of the second polar globule leading to the formation of the
431 female gamete only takes place at fertilization [29]. In males, meiosis is a continuous process taking
432 place in the post-natal period, just before puberty and resulting in the formation of four male gametes
433 from one spermatocyte. Despite these sex-dimorphic differences, the first reductional division of
434 meiosis is highly conserved between species and between sexes in terms of morphology and genetic
435 regulation. It was hypothesized that the mechanisms regulating and controlling prophase I during
436 mammalian meiosis, frequently named "checkpoints", are more stringent in males than in females.
437 This has been demonstrated over the last 25 years by the use of a large number of mutant mouse
438 models, mainly gene knockout mice [30–32].

439 A major checkpoint in males is the synaptic checkpoint that controls the zygotene-pachytene
440 transition, highlighted in male mice lacking *Sycp3*, *Dmc1*, *Spo11*, *mei1*, *Msh4-5* or *OvoL1* genes [33–
441 40]. In mutant females, this synaptic checkpoint is less stringent. Indeed, female meiotic arrest may
442 occur later, starting from the diplotene, as seen in *Dmc1*, *mei1*, *Msh4-5* knockout mice, during the
443 dictyate-resting phase of the oocyte, evidenced *Spo11*. These female mice can even be fertile, as seen
444 in *OvoL1* knockout mouse [40]. Other gene suppressions have highlighted a second meiotic checkpoint
445 of metaphase I in male, such as those of *Mlh1-3*, or cyclin A1, due to a misalignment of chromosomes
446 on the spindle [41–43]. Mice devoid of *Topaz1* gene could match these latter models. Indeed, *Topaz1*$^{-/-}$

447 spermatocytes do not progress to metaphase I and the chromosomes are not properly aligned on the
448 metaphase plate.
449
450 **TOPAZ1 seems to be involved in the cellular shape, structure and movements.**
451 The absence of *Topaz1* gene disturbs the transcriptome of the murine testes as early as 16 days
452 postnatal. Of the 205 DEGs at P16, 85 are specific to this stage of development compared to P18 (Fig
453 1A), such as *Ptgs1* (*Cox1*), marker of peritubular cells [44] and *Krt18*, marker of Sertoli cell maturation
454 [45]. Moreover, different genes involved in the TGFβ pathway are also P16-DEGs such as *Bmpr1b*, *Amh*,
455 *Fstl3*. This last one, for example, was demonstrated to reduce the Sertoli cells numbers in mouse testis
456 and to limit the organ size testis [46]. *Ptgds* (L-*Pgds*) playing a role in the PGD2 molecular pathway in
457 mammalian testicular organogenesis is also deregulated [47]. All these genes specifically deregulated
458 at P16 due to the absence of *Topaz1* thus seem to participate in the regulation of cell communication.
459 At P18, these genes are no longer differential, but genes belonging to the same gene families can
460 replace them, such as cadherin or keratin families for example.
461 Many of the 205 DEGs at P16 are involved in the defense response pathways. For example, *Ifit3* and
462 *Gbp3* are immune response genes in spermatocyte-derived GC-2spd(ts) cell [48].
463 Two days later, at P18, just before the prophase I-metaphase 1 transition, 10 times more genes are
464 deregulated. Among the 120 DEGs common to P16 and P18, there is at least one gene that may be
465 involved in meiosis such as *Aym1*, activator of yeast meiotic promoters 1. The absence of *Topaz1* leads
466 to the absence of testicular expression of *Aym1*. This gene is germ cell-specific [49]. In male mice, *Aym1*
467 is expressed from 10 d*pp* in early meiotic spermatocytes. The small murine AYM1 protein (44 amino
468 acids) is immunolocalized in the nucleus of primary spermatocytes, mainly late pachytene and
469 diplotene, suggesting a nuclear role of AYM1 in germ cells in first meiotic division[49].
470 At P18, the testicular transcriptome of *Topaz1*$^{-/-}$ mice is largely disturbed compared to WT and most
471 of DEGs are down-regulated (Fig 1F), suggesting that TOPAZ1 promotes gene expression in normal
472 mice. As TOPAZ1 is predicted to be an RNA-binding protein, it is tempting to speculate that its absence

473 disorganized ribonucleic-protein complexes, including their instabilities and degradation. This could
474 partly explain why 90% of DEGs are down-regulated at P18 with a large proportion of lincRNAs. These
475 down-regulated genes at P18 referred to microtubule-based movement and microtubule-based
476 process and cellular components refer to motile cilium, ciliary part, sperm flagellum, axoneme. In
477 addition, DAVID analysis revealed GO terms such as centriole, microtubule and spermatogenesis. All
478 these terms relate to elements of the cytoskeleton, which are indispensable for mitotic and/or meiotic
479 divisions, motility, differentiation and are also widely involved in spermiogenesis, as would be
480 expected with this latter GO terms since most DEGS are testis-specific. Centriole is a widely conserved
481 organelle in most organisms. A pair of centrioles is located into the heart of the centrosome, and the
482 whole is grouped together as the main microtubule-organizing center (MTOC). Here, the staining of
483 the meiotic spindle and centrosomes shows a disturbance of these pathways (Fig 2 and S2 Fig). Such
484 abnormal metaphase-like chromosomes arranged in rosette instead of being neatly aligned at the cell
485 equator and such hemispindles centered in the spermatocytes have already been observed. For
486 example, aberrant prometaphase-like cells were observed in *Mlh1*- or *Meioc*-deficient testes (*Meioc* is
487 down-regulated by 1.51 fold in P18 in *Topaz1*$^{-/-}$ testis) [41,50]. These mutant mice have been described
488 with an arrest of male meiosis, testes devoid of haploid germ cells leading to male sterility like mice
489 lacking the *Topaz1* gene. In *Topaz1* Mlh1 is not a DEG.
490
491 During spermatogenesis, dysregulation of centrosomal proteins may affect meiotic division and
492 genome stability. The centriole proteins CEP126, CEP128, CEP63 are down-regulated (FC from 2.1 to
493 2.7 compared to WT) at P18 in *Topaz1*$^{-/-}$ testis. CEP126 is localised with γ-tubulin on centriole during
494 mitosis of hTERT-RPE-1, human telomerase-immortalized retinal pigmented epithelial [51] but has
495 never been studied in germ cells during meiosis. CEP128 was localized to the mother centriole and
496 required for regulating ciliary signalling in zebrafish [52]. *Cep128* deletion decreased the stability of
497 centriolar microtubules in F9 cells (epithelial cells from testicular teratoma of mouse embryo) [53].
498 Normally, centriole separation occurs at the end of the prophase I or in early metaphase I and CEP63

499 is associated with the mother centrioles. The mouse model devoid of *Cep63* lead to male infertility
500 [54]. In spermatocytes of these mice, the centriole duplication was impaired. Finally, the ontology
501 analysis of *Topaz1*$^{-/-}$ P18-DEGs revealed significant enrichment score for the several clusters referred
502 to the spermatozoa final structure, like tetratricopeptide repeat (TPR) and dynein heavy chain
503 (DNAH1). Dynein chains are macromolecular complexes connecting the central pair or doublet pairs of
504 microtubules together to form the flagellar axoneme, the motility apparatus of spermatozoa (ref in
505 [55]). Dynein proteins have also been identified and involved in microtubule-based, intracellular
506 transport of vesicles, and in both mitosis and meiosis [56].
507 The TPR or PPR (pentatricopeptide repeat) domains consist of several 34 or 36 amino acid repeats
508 respectively constituting αα-hairpin repeat units [57]. The functions of TPR or PPR proteins were firstly
509 documented in plants and are involved in RNA editing [57,58]. In mouse, *Cfap70*, a tetratricopeptide
510 repeat-containing gene was shown to be expressed in the testis [59], or as *Spag1* rather in late-
511 pachytene spermatocytes or round spermatids [60]. Moreover, knockout mouse for *Ttc21a* shown
512 sperm structural defects of the flagella and the connecting piece. In human, *Ttc21a* was associated
513 with asthenoteratospermia in the Chinese population [61]. Many components of the intraflagellar
514 transport (IFT) complex contain TPR. Several genes coding for such tetratricopeptide repeat-containing
515 proteins are down-regulated in the P18 testis devoid of *Topaz1* like *Cfap70*, *Spag1*, *Tct21a*, *Ift140*.
516 Based on TPRpred [62], that predicted TPR- or PPR-containing proteins, the TOPAZ1 protein was
517 predicted to contain such domains, 7 in mice (p-val= 7.5E-08, probability for being PPR= 46.80%) and
518 10 in humans (p-val= 3.4E-09, probability for being PPR = 88.76%).
519 A recent study of single cell-RNA-seq from all types of homogeneous spermatogenetic cells identified
520 clusters of cells at similar developmental stages [63]. This study shown that most of genes involved in
521 spermiogenesis begin to be expressed from the early pachytene stage. This is consistent with our RNA-
522 seq results. Together, these data indicated that the absence of *Topaz1* down-regulated a significant
523 number of cytoskeleton-related genes which leads to a defect in the formation of the meiotic spindle
524 and to a deficient duplication and/or migration of centrosomes as early as 18 days post-natal. *Topaz1*

525 could lead to impaired chromosome dynamics via activation of cytoskeleton-genes and thus shows an
526 essential role for centrosome in promoting division and then fertility. The action of TOPAZ1 could be
527 carried out via its TPR domains.
528
529 **Topaz1 ablation deregulates a high proportion of lncRNAs**
530 DEGs between *Topaz1*$^{-/-}$ and WT mouse testes shown also a high proportion of deregulated lncRNAs.
531 We showed that three lincRNAs, whose expression is almost abolished as early as P16 in mouse
532 testicles lacking *Topaz1*, are testis- and germ cell-specific. We have shown that these genes are
533 expressed in spermatocytes and round spermatids suggesting a role in spermatogenesis. Their
534 functions are unknown.
535 Several investigations revealed that the testis is an organ allowing the expression of many lncRNAs
536 [64]. In mammals, the testis is the organ with the highest transcription rate [65]. However, during the
537 long stage of prophase I, the levels of transcription are not consistent. Indeed, transcription is strongly
538 reduced or even abolished in the entire nucleus of the spermatocytes during the early beginning of
539 prophase I. This is accompanied in particular by the nuclear processes of DNA division, pairing
540 homologous chromosome, telomeric rearrangement [66–68] and also by the onset of the MSCI,
541 meiotic sex chromosome inactivation, markers [69]. These processes are supported by epigenetic
542 changes such as histone modifications, recruitment of specific histone variants (references in Page et
543 al., 2012). Then, transcription takes up an important part in the late-pachytene until diplotene
544 spermatocytes [70]. The above-mentioned scRNA-seq study from individual spermatogenic cells
545 shown that almost 80% of annotated autosomal lncRNAs were expressed in spermatogenetic cells,
546 mainly from the mid-pachytene- to the metaphase I-spermatocytes but also in round spermatids [63].
547 The three lncRNAs investigated in our study (*4930463O16Rik, Gm21269* and *4921513H07Rik*) are also
548 expressed at these stages of development in the mouse testes [71,72]. In this last mentioned study
549 [72], the authors identified certain male germline-associated lncRNAs as potentially important for
550 spermatogenesis *in vivo*, based on several computational and experimental data sets. Among them

551 are *Gm21269* and *4921513H07Rik*. The localization of the lncRNAs in cells may be an indicator of their
552 potential function [73]. *4930463O16Rik* is expressed in the nucleus of spermatocytes. As mentioned
553 above, *4930463O16Rik* could have a positive role on the expression of *cKap4* at the neighboring locus.
554 Some nuclear lncRNA show transcription regulation with *cis*-regulatory role, such as *Malat1* or *Air*
555 [74,75] on their nearby gene. Other nuclear lncRNAs act in *trans* and regulate gene transcription at
556 another locus, such as *HOTAIR* [76]. In addition, some cytoplasmic lncRNA have been shown to play a
557 role in miRNA competition as miRNA sponges or decoys (such as *linc-MD1* in human myoblasts [77]).
558 *Gm21269* is localized in the cytoplasm and nuclei of spermatocytes during meiosis. Both cytoplasmic
559 and nuclear lncRNAs may act as molecular scaffold to assemble functional protein complexes, as
560 *HOTAIR* or *Dali* [78,79], to regulate protein localization and/or direct protein degradation, or as miRNA
561 precursor [80]. Finally, multiple other roles can be observed for lncRNAs. For example, the *Dali* lincRNA
562 locally regulates his neighboring *Pou3f3* gene, acts as a molecular scaffold for POU3F3 protein and
563 interacts with DNMT1 for regulation of DNA methylation status of CpG island-associated promoters in
564 *trans* during neural differentiation [79].
565

566 **Deletion of one lncRNA alters sperm parameters without affection fertility**

567 To decipher the biological function of a lncRNA affected by *Topaz1* invalidation, mouse model devoid
568 of *4930463O16Rik* were produced, under the same genetic background as for *Topaz1*$^{-/-}$ mice. This
569 knockout, did not disturb the meiosis and fertility of the mutant mice under standard laboratory
570 conditions. On a similar approach, *Sox30* is a testis-specific factor indispensable to obtain haploid germ
571 cells during spermatogenesis [81]. SOX30 regulates *Dnajb8* expression. However, deletion of *Dnajb8* is
572 not essential for spermatogenesis and male fertility [82].
573 Several mutant mouse deprived of testis-specific genes proved to be fertile, without any role being
574 stated during spermatogenesis. This was noted in particular for the *Flacc1*, *Trim69*, *Tex55*,
575 *4930524B15Rik* genes [83–86] or for highly testis-enriched genes like *Kdm4d*, *Tex37*, *Ccdc73* or *Prss55*
576 [87,88]. Some of them are down-regulated genes in *Topaz1*$^{-/-}$ or *4930463O16Rik*$^{-/-}$ testis (*Trim69* in

577 *Topaz1*$^{-/-}$ FC = 3.99 and in *4930463O16Rik*$^{-/-}$ FC = 2.27; *Kdm4d* in *Topaz1*$^{-/-}$ FC = 2.70 and in
578 *4930463O16Rik*$^{-/-}$ FC = 1.83; *Ccdc73* in *Topaz1*$^{-/-}$ FC = 1.46). Recently, some laboratories have also
579 generated several dozen of testis-enriched knockout mouse lines using the CRISPR/Cas9 system and
580 shown that all these genes are individually dispensable for male fertility in mice [89,90].
581 The abundant expression of lncRNAs during spermatogenesis has also prompted other laboratories to
582 perform knockout mouse model of testis-specific lncRNAs. This is the case for the *1700121C10Rik* or
583 *lncRNA5512* lncRNAs where mutant mice were also fertile without variation in sperm parameters
584 [91,92]. One working hypothesis could be that some lncRNAs might be regulators of subset of
585 functional spermatogenetic-gene expression, in agreement with their nuclear localization, by binding
586 to their regulatory genomic region.
587 Nevertheless, in our *4930463O16Rik*-knockout mouse model, several sperm parameters were altered,
588 including a reduction of epididymal sperm concentration by more than half and sperm motility. In the
589 *Tslrn1* knockout mice, testis-specific long non-coding RNA 1, males are fertile, showed a significant
590 20% sperm reduction, but no reduction in litter size or major defects in testis histology or variation of
591 sperm motility [93]. In *Kif9*-mutant male mice, no testis abnormalities were found [94]. They were
592 subfertile due to impaired sperm motility: the velocity parameters VSL and VAP were reduced, like in
593 the *4930463O16Rik* knockout mice. The authors concluded that *Kif9* mutant mice were still fertile
594 probably due to variations in the motility of individual spermatozoa. These spermatozoa with good
595 motility could still fertilize oocytes. The same conclusion could apply to mice *4930463O16Rik*$^{-/-}$.
596 Suppression of a gene, in this case the *4930463O16Rik* lincRNA, whose expression is highly down-
597 regulated in the testes of sterile *Topaz1*$^{-/-}$ mice (FC = 40), has no effect on spermatogenesis. Our data
598 suggest that the expression of *4930463O16Rik* is dispensable for meiotic divisions, but add to the
599 terminal differentiation of male germ cells.
600
601 Various genes, testis-specific or highly expressed in the testis, show no effect on reproduction when
602 deleted independently [90,91]. One explanation, given the large number of lncRNAs expressed in the

603 meiotic testis, could be that the function of *4930463O16Rik* is partly redundant with that of other
604 testicular lncRNAs.
605 However, outside the laboratory, in wild reproductive life, we could imagine that biological functions
606 in more natural conditions could be different due to stress and reproductive competition. This has
607 been shown in particular for *Pkdrej*-deficent male mice which are fertile, whereas the *Pkdrej* gene,
608 polycystin family receptor for egg jelly, is important in postcopulatory reproductive selection [90,95].
609
610 The absence of a specific anti-TOPAZ1 antibody does not allow us to futher advance in the
611 understanding of its function during murine spermatogenesis. The creation of a Flag-tagged *Topaz1*
612 knockin mouse model will allow us to get deeper inside. Rip-seq experiments will allow us to determine
613 RNA-TOPAZ1 complexes during spermatogenesis.
614
615

616 ## Materials and methods

617 ### Ethics statement

618 All animal experiments were performed in strict accordance with the recommendations in the
619 guidelines of the Code for Methods and Welfare Considerations in Behavioral Research with Animals
620 (Directive 2016/63/UE). Experiments were approved by the INRAE local animal experiment ethics
621 committee of Jouy-en-Josas (Comethea, number 18-12) and authorization issued from the French
622 Ministry of Higher Education, Research and Innovation (Number 815-2015073014516635).
623

624 ### Mice

625 Generation and preliminary analysis of the *Topaz1*-null transgenic mouse line was previously described
626 (Luangpraseuth-Prosper *et al*. 2015).

627 The generation of 4630493O16Rik-null transgenic mouse line was obtained using the CrispR-Cas9
628 genome editing technology. RNA mix comprising an mRNA encoding for the SpCas9-HF1 nuclease and
629 the four sgRNA (S4 Table) targeting the *4930463o16Rik* gene (NC_000076: 84324157-84333540) were
630 prepared. These sgRNAs were chosen following the CRISPOR software (http://crispor.tefor.net/) in
631 order to remove the 4 exons and introns of the *4930463o16Rik* gene. Cas9-encoding mRNA and the 4
632 sgRNAs were injected at 100 ng/µL each into 1 cell-fertilized C57Bl/6N mouse eggs [96].
633 Surviving injected eggs were transferred into pseudo-pregnant recipient mice. Tail-DNA analysis of the
634 resulting alive pups was performed by PCR using genotyping oligonucleotides (S4 Table) and Takara Ex
635 Taq® DNA Polymerase kit. PCR conditions were 94 °C 30s, 60 °C 30s and 72 °C 30s with 35 amplification
636 cycles.
637 Two transgenic founder mice were crossed with wild-type C57Bl/6N mice to establish transgenic lines.
638 F1 heterozygote mice were crossed together in each line to obtained F2 homozygote mice, thus
639 establishing the 4630493O16Rik$^{-/-}$ mouse lines. Both mouse lines were fertile, the number of pups was
640 equivalent, so we worked with one mouse line.
641 All mice were fed *ad libitum* and were housed at a temperature of 25°C under a 12h/12h light/dark
642 cycle at the UE0907 unit (INRAE, Jouy-en-Josas, France). Mice were placed in an enriched environment
643 to improve their reception while respecting the 3R. All mice were sacrificed by cervical dislocation.
644 Tissues at different developmental stages were dissected and fixed as indicated later or flash frozen
645 immediately in liquid nitrogen before storage at -80°C. Frozen tissues were used for molecular biology
646 experiments described later.
647

648 **Histological and immunohistochemical analyses**

649 For histological studies, fresh tissues from 8-week-old mice were fixed in 4% paraformaldehyde
650 (Electron Microscopy Sciences reference 50-980-495) in phosphate buffer saline (PBS) at 4°C. After
651 rinsing tissues in PBS, they were stored in 70% ethanol at 4°C. Then, paraffin inclusions were performed
652 with a Citadel automat (Thermo Scientific Shandon Citadel 1000) with standard protocol. Tissues

653 including in paraffin blocks were sectioned at 4µm and organized on Superfrost Plus Slides (reference
654 J1800AMNZ). Once dry, slides were stored at 4°C. On the day of the experiment, these slides with the
655 sectioned tissues were deparaffinized and rehydrating in successive baths of xylene and ethanol at
656 room temperature. For histology, testis sections were stained with hematoxylin and eosin (HE) by the
657 @Bridge platform (INRAE, Jouy-en-Josas) using an automatic Varistain Slide Stainer (Thermo Fisher
658 Scientific). To determine the seminiferous epithelium stages, we used periodic acid-Schiff staining
659 (PAS).
660 *In situ* hybridization experiments were performed using the RNAscope® system (ACB, Bio-Techne SAS,
661 Rennes, France). Briefly, probes (around 1000 nt long) for *Topaz1* (NM_001199736.1), *4930463o16Rik*
662 (NR_108059.1), *Gm21269* (NR_102375.1) and *4921513H07Rik* (NR_153846.1) were designed by the
663 ACB company and referenced with catalog numbers 402321, 431411, 549421 and 549441 respectively.
664 Negative and positive control were ordered from ACD with *Bacillus subtilis* dihydrodipicolinate
665 reductase (dapB) and *Homo sapiens* ubiquitin C (Hs-UBC) respectively. Hybridization was performed
666 according to the manufacturer's instructions using the labelling kit (RNAscope® 2.5HD assay-brown).
667 Brown labelling slides were counterstained PAS staining protocol and then, were observed as visible
668 signal. Hybridization was considered as positive when at least one dot was observed in one cell.
669 Colored sections were scanned using a 3DHISTECH panoramic scanner at the @Bridge platform (INRAE,
670 Jouy-en-Josas) and were analyses with Case Viewer software (3DHISTECH). We also used the
671 RNAscope® 2.5HD assay-red kit in combination with immunofluorescence in order to achieve
672 simultaneous visualization of RNA and protein on the same slide. In this way, the *IS*H protocol was
673 stopped with water immersion before hematoxylin counterstain. Instead, slides were washed in PBS
674 at room temperature. Mouse on mouse (M.O.M.) kit (BMK-2202, Vector laboratories) was used and
675 slides were incubated one hour in Blocking Reagent, 5 minutes in Working solution and 2 hours with a
676 primary antibody: DDX4 (ab13840, Abcam) or γH2AX(Ser139) (Merck), diluted at 1:200 in Blocking
677 Reagent. Detection was performed by using secondary antibody conjugated to DyLight 488 (green,
678 KPL). Then, diluted DAPI (1:1000 in PBS) was applied during eight minutes on slides. Slides were

679 mounted with Vectashield Hard Set Mounting Medium for fluorescence H-1400 and images were
680 captured at the MIMA2 platform (https://www6.jouy.inrae.fr/mima2/,
681 https://doi.org/10.15454/1.5572348210007727E12) with an inverted ZEISS AxioObserver Z1
682 microscope equipped with an ApoTome slider, a Colibri light source, Axiocam MRm camera. Images
683 were analyzed with the Axiovision software 4.8.2 (Carl Zeiss, Germany).
684

685 **Total RNA extraction and Quantitative RT-PCR (RT-qPCR)**

686 Total RNAs from post-natal mouse testis or other organs were isolated using Trizol reagent. RNAs were
687 purified with RNeasy Mini kit (Qiagen) following manufactures instruction and DNAse-treated
688 (Qiagen). Quantification of total RNAs was realized with a Qbit® Fluorometric Quantitation. Maxima
689 First-Strand cDNA Synthesis Kit (Thermo Scientific) was used to reverse transcript RNA in cDNA. Step
690 One system with Fast SYBR™ Green Master Mix (Applied Biosystems, ThermoFisher France) was used
691 for qPCR. qPCR was performed in duplicates for all tested genes and results were normalized with
692 qBase+ software (Biogazelle) [97]. Gapdh, Ywahz and Mapk1 were used as reference genes. For each
693 experiment, median values were plotted with GraphPad Prism, and statistical analyses were
694 performed with KrusKall-Wallis test in R software (Rcmdr package (p-value<0.05)). Primer sequences
695 used for RT-qPCR were provided in S4 Table.
696

697 **RNA-sequencing**

698 Total RNA quality was verified on Agilent 2100 Bioanalyser (Matriks, Norway) and samples with a RIN>9
699 were made available for RNA-sequencing. This work has benefited from the platform and expertise of
700 the High-throughput Sequencing Platform of I2BC (Gif-sur-Yvette, Université Paris-Saclay, France) for
701 oriented library preparation (Illumina Truseq RNA Sample Preparation Kit) and sequencing (Paired-end
702 75 bp; NextSeq). More than 38 million of 75 bp paired-end reads per sample were generated.
703

704 **Transcriptomic analysis**

705 Sequence libraries were aligned with the Ensembl 95 genome, with TopHat [98], and gene table counts
706 were obtained by applying featureCounts to these alignments [99]. Data normalization and single-gene
707 level analysis of the differential expression were performed using the DESeq2 [100]. Some samples
708 were sequenced several months apart. A batch effect was observed after the computation of
709 hierarchical clustering of samples. In order to take this effect into account, we introduced the batch
710 number into the DESeq2 model, as well as the studied condition. Differences were considered
711 significant for Benjamini-Hochberg adjusted p-values < 0.05, and absolute fold change >2 (absolute
712 Log2FC>1) [101]. The RNA-seq raw data have been deposited through SRA Submission portal
713 (https://submit.ncbi.nlm.nih.gov/subs/sra/) BioProject ID PRJNA698440.
714

715 **Biotype determination of DEGs**

716 Data available on the websites of NCBI, MGI (http://www.informatics.jax.org) and Ensembl
717 (https://www.ensembl.org/) were used simultaneously to determine the DEG biotypes. For this
718 purpose, the mouse genome information were obtained by ftp from NCBI
719 (ftp://ftp.ncbi.nih.gov/gene/DATA/GENE_INFO/Mammalia/Mus_musculus.gene_info.gz); the
720 annotation BioMart file from Ensembl (http://www.ensembl.org/biomart/martview; Ensembl genes
721 99, Mouse genes GRCm28.p6) and the feature types from MGI
722 (http://www.informatics.jax.org/marker/; with protein coding gene, non-coding RNA gene,
723 unclassified gene and pseudogenic region). Only data corresponding to DEGs were conserved. The files
724 from these three databases were therefore cross-referenced to determine the biotype of DEGs. When
725 the biotype of a gene was different between the databases, the annotation was then listed as genes
726 with "biotype conflict".
727

728 **Gene ontology enrichment**

729 Identified mouse DEGS were analyzed with Gene Ontology (GO) and Kyoto Encyclopedia of Genes and
730 Genomes (KEGG) pathway membership with Database performed using the DAVID Bioinformatic
731 Database 6.8 (https://david.ncifcrf.gov/). These analyses and pathways were considered significant for
732 a Benjamini corrected enrichment p-value of less than 0.05. Mouse Atlas Genome of differentially
733 expressed genes extracted from this study was performed via the Enrichr website
734 (https://maayanlab.cloud/Enrichr/).
735

736 **Sperm analysis**

737 Evaluation of the semen concentration and motility of WT and *4930463O16Rik*$^{-/-}$ 8-week-old mice were
738 realized by using the IVOS II Computer Assisted Sperm Analysis (CASA) system (Hamilton Thorne,
739 Beverly, MA, USA). The both fresh cauda epididymis per individual were removed and plunged into
740 200 µL of TCF buffer (Tris, citrate and fructose buffer) where they were chopped with small scissors.
741 For sperm release, the samples were incubated 10 minutes at 37°C. A 4 µl aliquot was placed in a
742 standardized four-chamber Leja counting slide (Leja Products B.V., Nieuw-Vennep, the Netherlands).
743 Ten microscope fields were analyzed using the predetermined starting position within each chamber
744 with an automated stage. Statistical analyses were performed using the mean of the 10 analysed fields
745 with at least 300 cells. The IVOS settings chosen was those defined for mice sperm-cell analysis (by
746 Hamilton Thorne). The principal parameters were fixed as follows: 45 frames were captured at 60 Hz.
747 Concerning the cell detection, the camera considered a signal as a spermatozoon when the elongation
748 percentage was between 70 (maximum) and 2 (minimum); the minimal brightness of the head at 186,
749 and the minimum and maximum size of the head at 7 and 100 µm² respectively. Used kinematic
750 thresholds were: cell travel max at 10µm, progressive STR at 45%, progressive VAP at 45µm/s, slow
751 VAP at 20µm/s, slow VSL at 30µm/s, static VAP at 4µm/S and static VSL at 1µm/s. The full settings used
752 was listed in S7 Table. The recorded CASA parameters included the average path velocity (VAP in
753 µm/s), straight line velocity (VSL in µm/s), curvilinear velocity (VCL in µm/s), amplitude of lateral head
754 displacement (ALH in µm), motility (percentage), and sperm concentration (.10^6/mL). The slow cells

755 were recorded as static. Median and interquartile range were plotted with GraphPad. To compare the
756 sperm parameters between WT and *4930463O16Rik*$^{-/-}$ mice, statistical analyses were performed with
757 the Kruskal-Wallis non-parametric test.
758

759 ## Acknowledgments

760 We warmly thank Jean-Luc Vilotte for allowing lncRNA deletion to take place in his laboratory, also for
761 the proofreading of this manuscript and for English corrections. We would like to thank the TACGENE
762 facility within the U1154-UMR7196, MNHN, Paris, especially Anne De Cian and Jean-Paul Concordet,
763 for the synthesis of gRNAs and Cas9 mRNA. We are grateful to all the members of our mouse
764 experimental unit (IERP, INRA, Jouy en Josas, France). We thank the @Bridge plateform for Agilent
765 Bioanalyzer using and for the histology facility (UMR 1313 GABI, Jouy-en-Josas, France), particularly,
766 Marthe Vilotte, for HE staining. We also thank the MIMA2 platform for providing access to the virtual
767 slide scanner (Panoramic SCAN, 3DHISTECH). We are grateful to all the members of the "Gonad
768 Differentiation and its Disturbances" team for our scientific and technical exchanges on Monday
769 mornings either in person or by videoconference.
770

771 ## References

772 1. Kleckner N. Meiosis: how could it work? Proc Natl Acad Sci U S A. 1996;93: 8167–8174.
773 doi:10.1073/pnas.93.16.8167

774 2. Luangpraseuth-Prosper A, Lesueur E, Jouneau L, Pailhoux E, Cotinot C, Mandon-Pépin B.
775 TOPAZ1, a germ cell specific factor, is essential for male meiotic progression. Dev Biol.
776 2015;406: 158–171. doi:10.1016/j.ydbio.2015.09.002

777 3. Baillet A, Le Bouffant R, Volff JN, Luangpraseuth A, Poumerol E, Thépot D, et al. TOPAZ1, a
778 novel germ cell-specific expressed gene conserved during evolution across vertebrates. PLoS
779 One. 2011;6: e26950. doi:10.1371/journal.pone.0026950

780 4. Brannan CI, Dees EC, Ingram RS, Tilghman SM. The product of the H19 gene may function as
781 an RNA. Mol Cell Biol. 1990;10: 28–36. doi:10.1128/mcb.10.1.28

782 5. Brockdorff N, Ashworth A, Kay GF, McCabe VM, Norris DP, Cooper PJ, et al. The product of the
783 mouse Xist gene is a 15 kb inactive X-specific transcript containing no conserved ORF and
784 located in the nucleus. Cell. 1992;71: 515–526. doi:10.1016/0092-8674(92)90519-i

785 6. Gil R, Latorre A. Factors behind junk DNA in bacteria. Genes (Basel). 2012;3: 634–650.
786 doi:10.3390/genes3040634

787 7. ENCODE Project Consortium, Birney E, Stamatoyannopoulos JA, Dutta A, Guigó R, Gingeras TR,
788 et al. Identification and analysis of functional elements in 1% of the human genome by the
789 ENCODE pilot project. Nature. 2007;447: 799–816. doi:10.1038/nature05874

790 8. Carninci P, Kasukawa T, Katayama S, Gough J, Frith MC, Maeda N, et al. The transcriptional
791 landscape of the mammalian genome. Science. 2005;309: 1559–1563.
792 doi:10.1126/science.1112014

793 9. Morris KV, Mattick JS. The rise of regulatory RNA. Nat Rev Genet. 2014;15: 423–437.
794 doi:10.1038/nrg3722

795 10. Bie B, Wang Y, Li L, Fang H, Liu L, Sun J. Noncoding RNAs: Potential players in the self-renewal
796 of mammalian spermatogonial stem cells. Mol Reprod Dev. 2018;85: 720–728.
797 doi:10.1002/mrd.23041

798 11. Quan G, Li J. Circular RNAs: biogenesis, expression and their potential roles in reproduction. J
799 Ovarian Res. 2018;11: 9. doi:10.1186/s13048-018-0381-4

800 12. Yadav RP, Kotaja N. Small RNAs in spermatogenesis. Mol Cell Endocrinol. 2014;382: 498–508.
801 doi:10.1016/j.mce.2013.04.015

802 13. Jarroux J, Morillon A, Pinskaya M. History, Discovery, and Classification of lncRNAs. Adv Exp
803 Med Biol. 2017;1008: 1–46. doi:10.1007/978-981-10-5203-3_1

804 14. Necsulea A, Kaessmann H. Evolutionary dynamics of coding and non-coding transcriptomes.
805 Nat Rev Genet. 2014;15: 734–748. doi:10.1038/nrg3802

806 15. Sarropoulos I, Marin R, Cardoso-Moreira M, Kaessmann H. Developmental dynamics of
807 lncRNAs across mammalian organs and species. Nature. 2019;571: 510–514.
808 doi:10.1038/s41586-019-1341-x

809 16. Wen K, Yang L, Xiong T, Di C, Ma D, Wu M, et al. Critical roles of long noncoding RNAs in
810 Drosophila spermatogenesis. Genome Res. 2016;26: 1233–1244. doi:10.1101/gr.199547.115

811 17. Arun G, Akhade VS, Donakonda S, Rao MRS. mrhl RNA, a long noncoding RNA, negatively
812 regulates Wnt signaling through its protein partner Ddx5/p68 in mouse spermatogonial cells.
813 Mol Cell Biol. 2012;32: 3140–3152. doi:10.1128/MCB.00006-12

814 18. Anguera MC, Ma W, Clift D, Namekawa S, Kelleher RJ, Lee JT. Tsx produces a long noncoding
815 RNA and has general functions in the germline, stem cells, and brain. PLoS Genet. 2011;7:
816 e1002248. doi:10.1371/journal.pgen.1002248

817 19. Zhang L, Lu H, Xin D, Cheng H, Zhou R. A novel ncRNA gene from mouse chromosome 5 trans-
818 splices with Dmrt1 on chromosome 19. Biochem Biophys Res Commun. 2010;400: 696–700.
819 doi:10.1016/j.bbrc.2010.08.130

820 20. Drumond AL, Meistrich ML, Chiarini-Garcia H. Spermatogonial morphology and kinetics during
821 testis development in mice: a high-resolution light microscopy approach. Reproduction.
822 2011;142: 145–155. doi:10.1530/REP-10-0431

823 21. Huang DW, Sherman BT, Lempicki RA. Systematic and integrative analysis of large gene lists
824 using DAVID bioinformatics resources. Nat Protoc. 2009;4: 44–57.
825 doi:10.1038/nprot.2008.211

826 22. Huang DW, Sherman BT, Zheng X, Yang J, Imamichi T, Stephens R, et al. Extracting biological
827 meaning from large gene lists with DAVID. Curr Protoc Bioinformatics. 2009;Chapter 13: Unit
828 13.11. doi:10.1002/0471250953.bi1311s27

829 23. Darde TA, Sallou O, Becker E, Evrard B, Monjeaud C, Le Bras Y, et al. The ReproGenomics
830 Viewer: an integrative cross-species toolbox for the reproductive science community. Nucleic
831 Acids Res. 2015;43: W109-116. doi:10.1093/nar/gkv345

832 24. Darde TA, Lecluze E, Lardenois A, Stévant I, Alary N, Tüttelmann F, et al. The ReproGenomics
833 Viewer: a multi-omics and cross-species resource compatible with single-cell studies for the
834 reproductive science community. Bioinformatics. 2019;35: 3133–3139.
835 doi:10.1093/bioinformatics/btz047

836 25. Toyooka Y, Tsunekawa N, Takahashi Y, Matsui Y, Satoh M, Noce T. Expression and intracellular
837 localization of mouse Vasa-homologue protein during germ cell development. Mech Dev.
838 2000;93: 139–149. doi:10.1016/s0925-4773(00)00283-5

839 26. Han J, Zhang J, Chen L, Shen B, Zhou J, Hu B, et al. Efficient in vivo deletion of a large imprinted
840 lncRNA by CRISPR/Cas9. RNA Biol. 2014;11: 829–835. doi:10.4161/rna.29624

841 27. Johnson WH. The significance to bull fertility of morphologically abnormal sperm. Vet Clin
842 North Am Food Anim Pract. 1997;13: 255–270. doi:10.1016/s0749-0720(15)30339-x

843 28. Vedrenne C, Hauri H-P. Morphogenesis of the endoplasmic reticulum: beyond active
844 membrane expansion. Traffic. 2006;7: 639–646. doi:10.1111/j.1600-0854.2006.00419.x

845 29. Handel MA, Eppig JJ. Sexual dimorphism in the regulation of mammalian meiosis. Curr Top
846 Dev Biol. 1998;37: 333–358. doi:10.1016/s0070-2153(08)60179-9

847 30. Morelli MA, Cohen PE. Not all germ cells are created equal: aspects of sexual dimorphism in
848 mammalian meiosis. Reproduction. 2005;130: 761–781. doi:10.1530/rep.1.00865

849 31. Su Y, Li Y, Ye P. Mammalian meiosis is more conserved by sex than by species: conserved co-
850 expression networks of meiotic prophase. Reproduction. 2011;142: 675–687.
851 doi:10.1530/REP-11-0260

852 32. Handel MA, Schimenti JC. Genetics of mammalian meiosis: regulation, dynamics and impact
853 on fertility. Nat Rev Genet. 2010;11: 124–136. doi:10.1038/nrg2723

854 33. Yuan L, Liu JG, Zhao J, Brundell E, Daneholt B, Höög C. The murine SCP3 gene is required for
855 synaptonemal complex assembly, chromosome synapsis, and male fertility. Mol Cell. 2000;5:
856 73–83. doi:10.1016/s1097-2765(00)80404-9

857 34. Pittman DL, Cobb J, Schimenti KJ, Wilson LA, Cooper DM, Brignull E, et al. Meiotic prophase
858 arrest with failure of chromosome synapsis in mice deficient for Dmc1, a germline-specific
859 RecA homolog. Mol Cell. 1998;1: 697–705. doi:10.1016/s1097-2765(00)80069-6

860 35. Baudat F, Manova K, Yuen JP, Jasin M, Keeney S. Chromosome synapsis defects and sexually
861 dimorphic meiotic progression in mice lacking Spo11. Mol Cell. 2000;6: 989–998.
862 doi:10.1016/s1097-2765(00)00098-8

863 36. Romanienko PJ, Camerini-Otero RD. The mouse Spo11 gene is required for meiotic
864 chromosome synapsis. Mol Cell. 2000;6: 975–987. doi:10.1016/s1097-2765(00)00097-6

865 37. Reinholdt LG, Schimenti JC. Mei1 is epistatic to Dmc1 during mouse meiosis. Chromosoma.
866 2005;114: 127–134. doi:10.1007/s00412-005-0346-4

867 38. Kneitz B, Cohen PE, Avdievich E, Zhu L, Kane MF, Hou H, et al. MutS homolog 4 localization to
868 meiotic chromosomes is required for chromosome pairing during meiosis in male and female
869 mice. Genes Dev. 2000;14: 1085–1097.

870 39. Edelmann W, Cohen PE, Kneitz B, Winand N, Lia M, Heyer J, et al. Mammalian MutS
871 homologue 5 is required for chromosome pairing in meiosis. Nat Genet. 1999;21: 123–127.
872 doi:10.1038/5075

873 40. Li B, Nair M, Mackay DR, Bilanchone V, Hu M, Fallahi M, et al. Ovol1 regulates meiotic
874 pachytene progression during spermatogenesis by repressing Id2 expression. Development.
875 2005;132: 1463–1473. doi:10.1242/dev.01658

876 41. Eaker S, Cobb J, Pyle A, Handel MA. Meiotic prophase abnormalities and metaphase cell death
877 in MLH1-deficient mouse spermatocytes: insights into regulation of spermatogenic progress.
878 Dev Biol. 2002;249: 85–95. doi:10.1006/dbio.2002.0708

879 42. Lipkin SM, Moens PB, Wang V, Lenzi M, Shanmugarajah D, Gilgeous A, et al. Meiotic arrest
880 and aneuploidy in MLH3-deficient mice. Nat Genet. 2002;31: 385–390. doi:10.1038/ng931

881 43. Liu D, Matzuk MM, Sung WK, Guo Q, Wang P, Wolgemuth DJ. Cyclin A1 is required for meiosis
882 in the male mouse. Nat Genet. 1998;20: 377–380. doi:10.1038/3855

883 44. Rey-Ares V, Rossi SP, Dietrich K-G, Köhn F-M, Schwarzer JU, Welter H, et al. Prostaglandin E2
884 (PGE2) is a testicular peritubular cell-derived factor involved in human testicular homeostasis.
885 Mol Cell Endocrinol. 2018;473: 217–224. doi:10.1016/j.mce.2018.01.022

886 45. Tarulli GA, Stanton PG, Lerchl A, Meachem SJ. Adult sertoli cells are not terminally
887 differentiated in the Djungarian hamster: effect of FSH on proliferation and junction protein
888 organization. Biol Reprod. 2006;74: 798–806. doi:10.1095/biolreprod.105.050450

889 46. Oldknow KJ, Seebacher J, Goswami T, Villen J, Pitsillides AA, O'Shaughnessy PJ, et al.
890 Follistatin-like 3 (FSTL3) mediated silencing of transforming growth factor β (TGFβ) signaling is
891 essential for testicular aging and regulating testis size. Endocrinology. 2013;154: 1310–1320.
892 doi:10.1210/en.2012-1886

893 47. Moniot B, Declosmenil F, Barrionuevo F, Scherer G, Aritake K, Malki S, et al. The PGD2
894 pathway, independently of FGF9, amplifies SOX9 activity in Sertoli cells during male sexual
895 differentiation. Development. 2009;136: 1813–1821. doi:10.1242/dev.032631

896 48. Kurihara M, Otsuka K, Matsubara S, Shiraishi A, Satake H, Kimura AP. A Testis-Specific Long
897 Non-Coding RNA, lncRNA-Tcam1, Regulates Immune-Related Genes in Mouse Male Germ
898 Cells. Front Endocrinol (Lausanne). 2017;8: 299. doi:10.3389/fendo.2017.00299

899 49. Malcov M, Cesarkas K, Stelzer G, Shalom S, Dicken Y, Naor Y, et al. Aym1, a mouse meiotic
900 gene identified by virtue of its ability to activate early meiotic genes in the yeast
901 Saccharomyces cerevisiae. Dev Biol. 2004;276: 111–123. doi:10.1016/j.ydbio.2004.08.026

902 50. Abby E, Tourpin S, Ribeiro J, Daniel K, Messiaen S, Moison D, et al. Implementation of meiosis
903 prophase I programme requires a conserved retinoid-independent stabilizer of meiotic
904 transcripts. Nat Commun. 2016;7: 10324. doi:10.1038/ncomms10324

905 51. Bonavita R, Walas D, Brown AK, Luini A, Stephens DJ, Colanzi A. Cep126 is required for
906 pericentriolar satellite localisation to the centrosome and for primary cilium formation. Biol
907 Cell. 2014;106: 254–267. doi:10.1111/boc.201300087

908 52. Mönnich M, Borgeskov L, Breslin L, Jakobsen L, Rogowski M, Doganli C, et al. CEP128 Localizes
909 to the Subdistal Appendages of the Mother Centriole and Regulates TGF-β/BMP Signaling at
910 the Primary Cilium. Cell Rep. 2018;22: 2584–2592. doi:10.1016/j.celrep.2018.02.043

911 53. Kashihara H, Chiba S, Kanno S-I, Suzuki K, Yano T, Tsukita S. Cep128 associates with Odf2 to
912 form the subdistal appendage of the centriole. Genes Cells. 2019;24: 231–243.
913 doi:10.1111/gtc.12668

914 54. Marjanović M, Sánchez-Huertas C, Terré B, Gómez R, Scheel JF, Pacheco S, et al. CEP63
915 deficiency promotes p53-dependent microcephaly and reveals a role for the centrosome in
916 meiotic recombination. Nat Commun. 2015;6: 7676. doi:10.1038/ncomms8676

917 55. Miyata H, Morohoshi A, Ikawa M. Analysis of the sperm flagellar axoneme using gene-
918 modified mice. Exp Anim. 2020;69: 374–381. doi:10.1538/expanim.20-0064

919 56. Mountain V, Compton DA. Dissecting the role of molecular motors in the mitotic spindle. Anat
920 Rec. 2000;261: 14–24. doi:10.1002/(SICI)1097-0185(20000215)261:1<14::AID-AR5>3.0.CO;2-E

921 57. D'Andrea LD, Regan L. TPR proteins: the versatile helix. Trends Biochem Sci. 2003;28: 655–
922 662. doi:10.1016/j.tibs.2003.10.007

923 58. Schmitz-Linneweber C, Small I. Pentatricopeptide repeat proteins: a socket set for organelle
924 gene expression. Trends Plant Sci. 2008;13: 663–670. doi:10.1016/j.tplants.2008.10.001

925 59. Shamoto N, Narita K, Kubo T, Oda T, Takeda S. CFAP70 Is a Novel Axoneme-Binding Protein
926 That Localizes at the Base of the Outer Dynein Arm and Regulates Ciliary Motility. Cells.
927 2018;7. doi:10.3390/cells7090124

928 60. Takaishi M, Huh N h. A tetratricopeptide repeat-containing protein gene, tpis, whose
929 expression is induced with differentiation of spermatogenic cells. Biochem Biophys Res
930 Commun. 1999;264: 81–85. doi:10.1006/bbrc.1999.1477

931 61. Liu W, He X, Yang S, Zouari R, Wang J, Wu H, et al. Bi-allelic Mutations in TTC21A Induce
932 Asthenoteratospermia in Humans and Mice. Am J Hum Genet. 2019;104: 738–748.
933 doi:10.1016/j.ajhg.2019.02.020

934 62. Karpenahalli MR, Lupas AN, Söding J. TPRpred: a tool for prediction of TPR-, PPR- and SEL1-like
935 repeats from protein sequences. BMC Bioinformatics. 2007;8: 2. doi:10.1186/1471-2105-8-2

936 63. Chen Y, Zheng Y, Gao Y, Lin Z, Yang S, Wang T, et al. Single-cell RNA-seq uncovers dynamic
937 processes and critical regulators in mouse spermatogenesis. Cell Res. 2018;28: 879–896.
938 doi:10.1038/s41422-018-0074-y

939 64. Necsulea A, Soumillon M, Warnefors M, Liechti A, Daish T, Zeller U, et al. The evolution of
940 lncRNA repertoires and expression patterns in tetrapods. Nature. 2014;505: 635–640.
941 doi:10.1038/nature12943

942 65. Soumillon M, Necsulea A, Weier M, Brawand D, Zhang X, Gu H, et al. Cellular source and
943 mechanisms of high transcriptome complexity in the mammalian testis. Cell Rep. 2013;3:
944 2179–2190. doi:10.1016/j.celrep.2013.05.031

945 66. Bolcun-Filas E, Schimenti JC. Genetics of meiosis and recombination in mice. Int Rev Cell Mol
946 Biol. 2012;298: 179–227. doi:10.1016/B978-0-12-394309-5.00005-5

947 67. Baudat F, Imai Y, de Massy B. Meiotic recombination in mammals: localization and regulation.
948 Nat Rev Genet. 2013;14: 794–806. doi:10.1038/nrg3573

949 68. Shibuya H, Watanabe Y. The meiosis-specific modification of mammalian telomeres. Cell
950 Cycle. 2014;13: 2024–2028. doi:10.4161/cc.29350

951 69. Page J, de la Fuente R, Manterola M, Parra MT, Viera A, Berríos S, et al. Inactivation or non-
952 reactivation: what accounts better for the silence of sex chromosomes during mammalian
953 male meiosis? Chromosoma. 2012;121: 307–326. doi:10.1007/s00412-012-0364-y

954 70. Monesi V. RIBONUCLEIC ACID SYNTHESIS DURING MITOSIS AND MEIOSIS IN THE MOUSE
955 TESTIS. J Cell Biol. 1964;22: 521–532. doi:10.1083/jcb.22.3.521

956 71. Chen Y, Zheng Y, Gao Y, Lin Z, Yang S, Wang T, et al. Single-cell RNA-seq uncovers dynamic
957 processes and critical regulators in mouse spermatogenesis. Cell Res. 2018;28: 879–896.
958 doi:10.1038/s41422-018-0074-y

959 72. Li K, Xu J, Luo Y, Zou D, Han R, Zhong S, et al. Panoramic transcriptome analysis and functional
960 screening of long noncoding RNAs in mouse spermatogenesis. Genome Res. 2021;31: 13–26.
961 doi:10.1101/gr.264333.120

962 73. Chen L-L. Linking Long Noncoding RNA Localization and Function. Trends Biochem Sci.
963 2016;41: 761–772. doi:10.1016/j.tibs.2016.07.003

964 74. Zhang B, Arun G, Mao YS, Lazar Z, Hung G, Bhattacharjee G, et al. The lncRNA Malat1 is
965 dispensable for mouse development but its transcription plays a cis-regulatory role in the
966 adult. Cell Rep. 2012;2: 111–123. doi:10.1016/j.celrep.2012.06.003

967 75. Sleutels F, Zwart R, Barlow DP. The non-coding Air RNA is required for silencing autosomal
968 imprinted genes. Nature. 2002;415: 810–813. doi:10.1038/415810a

969 76. Chu C, Qu K, Zhong FL, Artandi SE, Chang HY. Genomic maps of long noncoding RNA
970 occupancy reveal principles of RNA-chromatin interactions. Mol Cell. 2011;44: 667–678.
971 doi:10.1016/j.molcel.2011.08.027

972 77. Cesana M, Cacchiarelli D, Legnini I, Santini T, Sthandier O, Chinappi M, et al. A long noncoding
973 RNA controls muscle differentiation by functioning as a competing endogenous RNA. Cell.
974 2011;147: 358–369. doi:10.1016/j.cell.2011.09.028

975 78. Tsai M-C, Manor O, Wan Y, Mosammaparast N, Wang JK, Lan F, et al. Long noncoding RNA as
976 modular scaffold of histone modification complexes. Science. 2010;329: 689–693.
977 doi:10.1126/science.1192002

978 79. Chalei V, Sansom SN, Kong L, Lee S, Montiel JF, Vance KW, et al. The long non-coding RNA Dali
979 is an epigenetic regulator of neural differentiation. Elife. 2014;3: e04530.
980 doi:10.7554/eLife.04530

981 80. Cai X, Cullen BR. The imprinted H19 noncoding RNA is a primary microRNA precursor. RNA.
982 2007;13: 313–316. doi:10.1261/rna.351707

983 81. Bai S, Fu K, Yin H, Cui Y, Yue Q, Li W, et al. Sox30 initiates transcription of haploid genes during
984 late meiosis and spermiogenesis in mouse testes. Development. 2018;145.
985 doi:10.1242/dev.164855

986 82. Wang F, Kong S, Hu X, Li X, Xu B, Yue Q, et al. Dnajb8, a target gene of SOX30, is dispensable
987 for male fertility in mice. PeerJ. 2020;8: e10582. doi:10.7717/peerj.10582

988 83. Chotiner JY, Leu NA, Wang PJ. FLACC1 is testis-specific but dispensable for fertility in mice.
989 Mol Reprod Dev. 2020;87: 1199–1201. doi:10.1002/mrd.23435

990 84. He X, Xie W, Li H, Cui Y, Wang Y, Guo X, et al. The testis-specifically expressed gene Trim69 is
991 not essential for fertility in mice. J Biomed Res. 2020;35: 47–60. doi:10.7555/JBR.34.20200069

992 85. Jamin SP, Petit FG, Demini L, Primig M. Tex55 encodes a conserved putative A-kinase
993 anchoring protein dispensable for male fertility in the mouse. Biol Reprod. 2021.
994 doi:10.1093/biolre/ioab007

995 86. Khan R, Ye J, Yousaf A, Shah W, Aftab A, Shah B, et al. Evolutionarily conserved and testis-
996 specific gene, 4930524B15Rik, is not essential for mouse spermatogenesis and fertility. Mol
997 Biol Rep. 2020;47: 5207–5213. doi:10.1007/s11033-020-05595-0

998 87. Iwamori N, Zhao M, Meistrich ML, Matzuk MM. The testis-enriched histone demethylase,
999 KDM4D, regulates methylation of histone H3 lysine 9 during spermatogenesis in the mouse
1000 but is dispensable for fertility. Biol Reprod. 2011;84: 1225–1234.
1001 doi:10.1095/biolreprod.110.088955

1002 88. Khan M, Jabeen N, Khan T, Hussain HMJ, Ali A, Khan R, et al. The evolutionarily conserved
1003 genes: Tex37, Ccdc73, Prss55 and Nxt2 are dispensable for fertility in mice. Sci Rep. 2018;8:
1004 4975. doi:10.1038/s41598-018-23176-x

1005 89. Lu Y, Oura S, Matsumura T, Oji A, Sakurai N, Fujihara Y, et al. CRISPR/Cas9-mediated genome
1006 editing reveals 30 testis-enriched genes dispensable for male fertility in mice†. Biol Reprod.
1007 2019;101: 501–511. doi:10.1093/biolre/ioz103

1008 90. Miyata H, Castaneda JM, Fujihara Y, Yu Z, Archambeault DR, Isotani A, et al. Genome
1009 engineering uncovers 54 evolutionarily conserved and testis-enriched genes that are not

1010 required for male fertility in mice. Proc Natl Acad Sci U S A. 2016;113: 7704–7710.
1011 doi:10.1073/pnas.1608458113

1012 91. Li C, Shen C, Shang X, Tang L, Xiong W, Ge H, et al. Two novel testis-specific long noncoding
1013 RNAs produced by *1700121C10Rik* are dispensable for male fertility in mice. J Reprod Dev.
1014 2020;66: 57–65. doi:10.1262/jrd.2019-104

1015 92. Zhu Y, Lin Y, He Y, Wang H, Chen S, Li Z, et al. Deletion of lncRNA5512 has no effect on
1016 spermatogenesis and reproduction in mice. Reprod Fertil Dev. 2020;32: 706–713.
1017 doi:10.1071/RD19246

1018 93. Wichman L, Somasundaram S, Breindel C, Valerio DM, McCarrey JR, Hodges CA, et al. Dynamic
1019 expression of long noncoding RNAs reveals their potential roles in spermatogenesis and
1020 fertility. Biol Reprod. 2017;97: 313–323. doi:10.1093/biolre/iox084

1021 94. Miyata H, Shimada K, Morohoshi A, Oura S, Matsumura T, Xu Z, et al. Testis-enriched kinesin
1022 KIF9 is important for progressive motility in mouse spermatozoa. FASEB J. 2020;34: 5389–
1023 5400. doi:10.1096/fj.201902755R

1024 95. Sutton KA, Jungnickel MK, Florman HM. A polycystin-1 controls postcopulatory reproductive
1025 selection in mice. Proc Natl Acad Sci U S A. 2008;105: 8661–8666.
1026 doi:10.1073/pnas.0800603105

1027 96. Henao-Mejia J, Williams A, Rongvaux A, Stein J, Hughes C, Flavell RA. Generation of
1028 Genetically Modified Mice Using the CRISPR-Cas9 Genome-Editing System. Cold Spring Harb
1029 Protoc. 2016;2016: pdb.prot090704. doi:10.1101/pdb.prot090704

1030 97. Hellemans J, Mortier G, De Paepe A, Speleman F, Vandesompele J. qBase relative
1031 quantification framework and software for management and automated analysis of real-time
1032 quantitative PCR data. Genome Biol. 2007;8: R19. doi:10.1186/gb-2007-8-2-r19

1033 98. Trapnell C, Pachter L, Salzberg SL. TopHat: discovering splice junctions with RNA-Seq.
1034 Bioinformatics. 2009;25: 1105–1111. doi:10.1093/bioinformatics/btp120

1035 99. Liao Y, Smyth GK, Shi W. featureCounts: an efficient general purpose program for assigning
1036 sequence reads to genomic features. Bioinformatics. 2014;30: 923–930.
1037 doi:10.1093/bioinformatics/btt656

1038 100. Love MI, Huber W, Anders S. Moderated estimation of fold change and dispersion for RNA-
1039 seq data with DESeq2. Genome Biol. 2014;15: 550. doi:10.1186/s13059-014-0550-8

1040 101. Benjamini Y, Hochberg Y. Controlling the False Discovery Rate: A Practical and Powerful
1041 Approach to Multiple Testing. Journal of the Royal Statistical Society Series B
1042 (Methodological). 1995;57: 289–300.

1043

1044 ## Supporting information

1045 **S1 Fig. Validation of several DEGs by RT-qPCR (RNA-seq *Topaz1*$^{-/-}$ *vs* WT testes).**

1046 Validation of several differentially expressed up- or down-regulated genes and of non-DEGs of RNA-
1047 seq analysis by qRT-PCR from P16 (A) or P18 (B) mouse testis RNAs. The lines represent the median of
1048 each genotype (blue: WT; red: *Topaz1*$^{-/-}$). A statistical test of Kruskal-Wallis was carried out (*p<0.05).
1049
1050 **S2 Fig. Abnormal centrosome labelling in Topaz1-deficient gonads.**
1051 Immunofluorescence staining for γ-TUBULIN (red) and DAPI (blue) in WT (left) and *Topaz1*$^{-/-}$ (right) 30
1052 d*pp* testis sections. Unlike the two red dots locating centrosomes in the meiotic metaphases seen in
1053 normal testes (left), centrosomes are abnormal in *Topaz1*$^{-/-}$ mutants (right) with one diffuse labelling.
1054 Zooms in white squares showed spermatocytes in metaphase I (WT) or in metaphase I-like (*Topaz1*$^{-/-}$).
1055 Scale bar = 50µm
1056
1057 **S3 Fig. Reprogenomics data on dynamic expression of *4930463O16Rik*.**
1058 Dynamic expression of *4930463O16Rik* in five different tissues in male and female adult mice (A), in
1059 embryo primordial germ cells and adult male germ cells (B). *4930463O16Rik* is expressed in testis in
1060 germ cell during post-natal life. The strongest dynamic expression is found in pachytene
1061 spermatocytes.
1062
1063 **S4 Fig. Reprogenomics data on dynamic expression of *Gm21269*.**
1064 Dynamic expression of *Gm21269* in five different tissues in male and female adult mice (A), in embryo
1065 primordial germ cells and adult male germ cells (B). *Gm21269* is expressed in testis in germ cell during
1066 post-natal life. The strongest dynamic expression is found in pachytene spermatocytes.
1067
1068 **S5 Fig. IGV representation of P18-testis RNA-seq.**
1069 Expression of *4930463O16Rik* (A), *Gm21269* (B) and *4921513H07Rik* (C) from BigWig files of strand-
1070 specific RNA-seq data. The first four tracks represent transcripts of WT testes at P18; the next three
1071 tracks represent transcripts of *Topaz1*$^{-/-}$ testis at the same developmental stage.Representations of the

1072 genes (from mm10 or GRCm38) are at the bottom of each graph. At the top of each one, there is the
1073 representation of the size of *4930463O16Rik* (A), *Gm21269* (B) and *492151H07Rik* (C) transcripts (red)
1074 from Ensembl data (GRCm38). *4930463O16Rik* and *4921513H07Rik* gene transcriptions overlap in 3'
1075 or 5' respectively.
1076
1077 **S6 Fig. Expression of *Gm21269*, *4930463O16Rik* and *492151H07Rik* mRNAs in testes from 5 days to**
1078 **adulthood.**
1079 Quantitative RT-PCR analysis of *Gm21269*, *4930463O16Rik* and *492151H07Rik* gene expressions at
1080 different developmental stages in WT (blue) and *Topaz1*$^{-/-}$ (red) testes. The lines represent the median
1081 of each genotype. A statistical test of Kruskal-Wallis was carried out (*p<0.05; **p<0.01).
1082
1083 **S7 Fig. *IS*H with PAS counterstained in WT mouse testis.**
1084 Visualisation of 493O16Rik (A), *Gm21269* (B) and *4921513H07Rik* (C) mRNAs respectively by *IS*H at
1085 different seminiferous epithelium stages highlighted by PAS staining. Scale bar = 20µm
1086
1087 **S8 Fig. LncRNA cellular localizations on WT two month-old mouse testes.**
1088 *IS*H using (A) *4930463O16Rik*, (D) *Gm21269* and (G) *4921513H07Rik* probes (red). (B-E-H)
1089 Immunofluorescence staining with γH2Ax antibody was achieved in the same stage of seminiferous
1090 epithelium to identify male germ cells (green). (C-F-I) DAPI (blue), visualizing nuclear chromosomes,
1091 was merge with *IS*H (green) and IF (red) signals. Zooms in white squares showed spermatocytes during
1092 prophase I. No colocation between the sex body (γH2Ax) and lncRNAs (red) was evident. Scale bar =
1093 20 µm.
1094
1095 **S9 Fig. Validation of several DEGs by RT-qPCR (RNA-seq *4930463O16Rik*$^{-/-}$ *vs* WT testes).**
1096 Validation of several differentially expressed up- or down-regulated genes and of non-DEGs of RNA-
1097 seq analysis by RT-qPCR from P16 (A) or P18 (B) mouse testis RNAs. The lines represent the median of

1098 each genotype (blue: WT; red: 4930463O16Rik$^{-/-}$). A statistical test of Kruskal-Wallis was carried out
1099 (*p<0.05).
1100
1101 **S1 Table. List of DEGs in *Topaz1*$^{-/-}$ testis compared to WT.**
1102 List of deregulated genes in *Topaz1* KO testes at P16 (sheet 1) and P18 (sheet 2) (adjusted p-value <
1103 0.05 and absolute Log2FC>1).
1104
1105 **S2 Table. Functional annotation of P16 DEGs (RNA-seq *Topaz1*$^{-/-}$ *vs* WT testes)**.
1106 DAVID functional Annotation Clustering (DAVID 6.8) analysis (based on GO terms and KEGG pathway)
1107 of all P16-differentially expressed genes (sheet 1) or only up-regulated (sheet 2) or down-regulated
1108 DEGs (sheet 3) in *Topaz1*$^{-/-}$ testis.
1109
1110 **S3 Table. Functional annotation of P18 DEGs (RNA-seq *Topaz1*$^{-/-}$ *vs* WT testes)**.
1111 DAVID functional Annotation Clustering (DAVID 6.8) analysis (based on GO terms and KEGG pathway)
1112 of P18-differentially expressed genes (sheet 1) or only up-regulated (sheet 2) or down-regulated DEGs
1113 (sheet 3) in *Topaz1*$^{-/-}$ testis. Annotation clusters based on InterPro database of P18-down-regulated
1114 DEGs have been mentioned in sheet 4.
1115
1116 **S4 Table. List of primers.**
1117 List of different primers used in this study for genotyping, RT-qPCR and gRNAs).
1118
1119 **S5 Table. List of DEGs in *4930463O16Rik*$^{-/-}$ testis compared to WT.**
1120 List of deregulated genes in *4930463O16Rik* KO testes at P16 (sheet 1) and P18 (sheet 2) (adjusted p-
1121 value < 0.05 and absolute Log2FC>1).
1122
1123 **S6 Table. Functional annotation of P16 DEGs (RNA-seq *4930463O16Rik*$^{-/-}$ *vs* WT testes)**.

1124 DAVID functional Annotation Clustering (DAVID 6.8) analysis of P18-differentially expressed genes

1125 (sheet 1) or only up-regulated (sheet 2) or down-regulated DEGs (sheet 3) in *4930463O16Rik*$^{-/-}$ testis.

1126

1127 **S7 Table. Casa system settings.**

1128